Received: 30 September 2025 | Accepted: 7 January 2026

DOI: 10.1002/ecs2.70608

ECOSPHERE
AN ESA OPEN ACCESS JOURNAL

ARTICLE

Coastal and Marine Ecology

Synthetic pelagic biomass size spectra of the tropical and subtropical Atlantic

Heino O. Fock[1] | **Henrike Andresen**[1] | **Arnaud Bertrand**[2] | **Gabriel Bittencourt Farias**[3] | **Claire Carré**[2] | **María Couret**[4] | **Javier Díaz-Pérez**[4] | **Tim Dudeck**[5] | **Mathilde Dugenne**[6] | **Sabrina Duncan**[1] | **Gabriela Guerra Araújo Abrantes Figueiredo**[3] | **Thierry Frédou**[7] | **Flávia Lucena-Frédou**[7] | **Xiomara F. G. Díaz**[8] | **Dawit Yemane**[9] | **Cristina González-García**[10] | **Rainer Kiko**[11,12] | **José M. Landeira**[4,13] | **Simone M. A. Lira**[3] | **Florian Lüskow**[14] | **Emilio Marañón**[15] | **Pedro Augusto Mendes de Castro Melo**[3] | **Sigrid Neumann-Leitao**[3] | **Leandro Nole Eduardo**[2] | **Lars Stemmann**[6] | **Ralf Schwamborn**[3]

[1]Thünen Institute of Sea Fisheries, Bremerhaven, Germany

[2]MARBEC, University Montpellier, CNRS, IFREMER, IRD, Sète, France

[3]Department of Oceanography, Federal University of Pernambuco (UFPE), Recife, Brazil

[4]Universidad de Las Palmas de Gran Canaria, Instituto de Oceanografía y Cambio Global, Las Palmas, Spain

[5]Leibniz Centre for Tropical Marine Research (ZMT), Bremen, Germany

[6]Laboratory of Villefranche sur Mer, Sorbonne University, Villefranche-sur-Mer, France

[7]Department of Fisheries and Aquaculture, Universidade Federal Rural de Pernambuco (UFRPE), Recife, Brazil

[8]Universidade Federal Rural da Amazonia (UFRA), Instituto Socioambiental e dos Recursos Hídricos-Isarh, Belém, Brazil

[9]Department of Forestry, Fisheries & the Environment, Fisheries Branch, Cape Town, South Africa

[10]Instituto Español de Oceanografía, IEO-CSIC, Centro Oceanográfico de Vigo, Vigo, Spain

[11]GEOMAR Helmholtz Centre for Ocean Research, Kiel, Germany

[12]Faculty of Natural Sciences, Kiel University, Kiel, Germany

[13]Department of Biology, Norwegian University of Science and Technology, Trondheim, Norway

[14]Department of Earth, Ocean and Atmospheric Sciences and Institute for the Oceans and Fisheries, University of British Columbia, Vancouver, Canada

[15]Departamento de Ecología y Biología Animal, Universidade de Vigo, Vigo, Spain

Correspondence
Heino O. Fock
Email: heino.o.fock@web.de

Present address
Heino O. Fock, ecoanalysis.de
Königsberger Strasse 9, Bad Segeberg, Germany.

Abstract

Synthetic normalized biomass size spectra (NBSS) comprising non-synoptically sampled phytoplankton, meso- and macrozooplankton, and micronekton including mesopelagic fishes were explored to analyze pelagic community structure in seven regions of the tropical and the subtropical Atlantic representative of different water bodies (NE Brazil shelf, NE Brazil oceanic islands,

Funding information
Universidad de Las Palmas de Gran Canaria, Grant/Award Number: ULPGC2022-2; Center for Operational Oceanographic Products and Services, Grant/Award Number: NA21OAR4310254; Federal Ministry of Education and Research, Grant/Award Numbers: 03F0797A, 03F0797D; Spanish Ministry of Science and Technology, Grant/Award Number: PID 2020-118118RB-100; EU Framework Programme for Research and Innovation H2020, Grant/Award Number: 817578EU H2020; Agencia Canaria de Investigación, Innovación y Sociedad de la Información, Grant/Award Number: TESIS2022010116

Handling Editor: Robert J. Miller

northern and southern offshore Benguela Upwelling System, northern offshore Canary Current Upwelling System, equatorial region, southern Canary Current Upwelling System oxygen minimum zone). For mesopelagic fishes and micronekton, conversions were applied accounting for sampling biases in relation to other ecosystem components. Three main results were obtained. Firstly, NBSS slopes based on biovolume were significantly shallower than slopes based on carbon contents, as revealed in part through pairwise comparisons of linear models and by ANOVA. The ensemble mean slope for six regions combined (one region omitted due to missing zooplankton data) measured in terms of biovolume was −0.866, and the respective value in terms of carbon biomass was −0.894. Secondly, log ratios of spectral densities, that is, contrasts, between consumers and phytoplankton increased with decreasing primary production. Contrasts for total micronekton and mesopelagic fishes relative to phyto- and zooplankton varied with primary production, indicating that below a primary production of 650 mg C m^{-2} day^{-1}, their spectral densities were higher than predicted by phytoplankton. Above this level, however, the spectral densities were lower. Thirdly, regional population marginal means were positively correlated with primary production in terms of carbon biomass ($p = 0.01$) but not biovolume ($p = 0.48$). Biovolume NBSS slopes were negatively correlated with primary production ($p = 0.02$), if the northern Benguela Upwelling System was not included (else $p = 0.11$). The increase in biovolume relative to the carbon biomass of gelatinous organisms is discussed as allometric advantage to enhance trophic transfer efficiency. Trophic transfer efficiencies ranged from 28.9% to 36.8% for open-ocean systems and from 36.8% to 49.7% for coastal and oceanic island habitats. The results suggest that synthetic pelagic size spectra provide a powerful framework to detect regional and functional shifts in Atlantic pelagic communities, offering predictive value for future ocean changes under climate scenarios.

KEYWORDS
mesopelagic fishes, phytoplankton, size spectra analysis, underwater vision profiler, zooplankton

INTRODUCTION

Biomass distribution in marine ecosystems differs fundamentally from that in terrestrial systems, where heterotrophs represent only about 2% of the total biomass. In the oceans, by contrast, heterotrophic organisms account for more than 80% of the biomass (Bar-On & Milo, 2019). The hypothesis that marine biomass is distributed in roughly equal concentrations across body-size classes, from "phytoplankton to whales" (Sheldon et al., 1972; Sheldon & Parsons, 1967), provided the foundation for abundance–biomass allometry relationships and size spectra models that are among the most widely used empirical macroecological patterns to describe changes in the functioning of ecological communities (Cohen et al., 2003; Kerr & Dickie, 2001; Stemmann & Boss, 2012). The central premise is that community biomass (B) does not change with body mass (M) but is shaped by processes that govern energy flow between trophic levels (TLs). With bacteria and phytoplankton providing the basis of all marine pelagic food webs, size spectra properties certainly depend on how well the basal resources can be incorporated in the analysis. In marine systems, heterotrophic plankton biomass exceeds autotrophic biomass in both coastal and ocean habitats (Del Giorgio & Gasol, 1995; Gasol et al., 1997; Pomeroy et al., 2007). Accordingly, marine bacterioplankton biomass is higher than phytoplankton biomass, which leads

to "inverted" size distributions, where the biomass of autotrophic producers is less than that of herbivorous and bacterivorous zooplankton (Gasol et al., 1997; Lombard et al., 2024). Inverted biomass pyramids are typical of ecosystems where a consumer level has more than one energy source (Trebilco et al., 2013). The imbalance between heterotrophic and autotrophic plankton biomass is greater the more oligotrophic the environment is, leading to a negative correlation between the heterotrophic-to-autotrophic biomass ratio and primary production (Gasol et al., 1997). A second effect observed for marine zooplankton is the prevalence of gelatinous plankton in oceanic systems so that these systems have a relatively shallow size spectrum slope and become top-heavy, that is, with many large, volume-rich specimens, while systems with a strong dominance of autotrophic production and a stronger contribution of non-gelatinous plankton become bottom-heavy with steeper size spectra slopes (Kwong et al., 2022).

This has certain implications for the analysis and interpretation of size spectra from phytoplankton to fishes, described in the log–log form by means of their dimensions slope and intercept or elevation (Figure 1d; see Yvon-Durocher et al., 2011). Rodríguez (1994) and Guiet et al. (2016) identified how certain processes affect size spectrum dimensions, although effects may differ depending on ecosystem component and habitat (dos Santos et al., 2017). Growth and predation would tend to flatten slopes by redistributing biomass towards higher body mass classes. In turn, microbial turnover and production of dissolved organic matter (DOM) result in steeper slopes, by limiting transfer to higher levels. Coagulation makes this material accessible for larger detritivores, and heterotrophic incorporation by decomposers would in turn create shallow slopes. Increased autotrophic production would affect size spectrum intercepts positively, incorporating more biomass into the entire food chain, while respiration would have the opposite effect. Given that community biomass does not change with body mass M and the biomass spectrum thus scales as M^0 across all TLs, in normalized biomass size spectra (NBSS, i.e., division by M), biomass scales as M^{-1}, which is denoted as $B(M)$, the spectral density of biomass B at M. The Metabolic Theory of Ecology (MTE) predicts the slope to be composed of a term of −0.75 depending on metabolic constraints and a predation term with a value of −0.25 regulated through a transfer

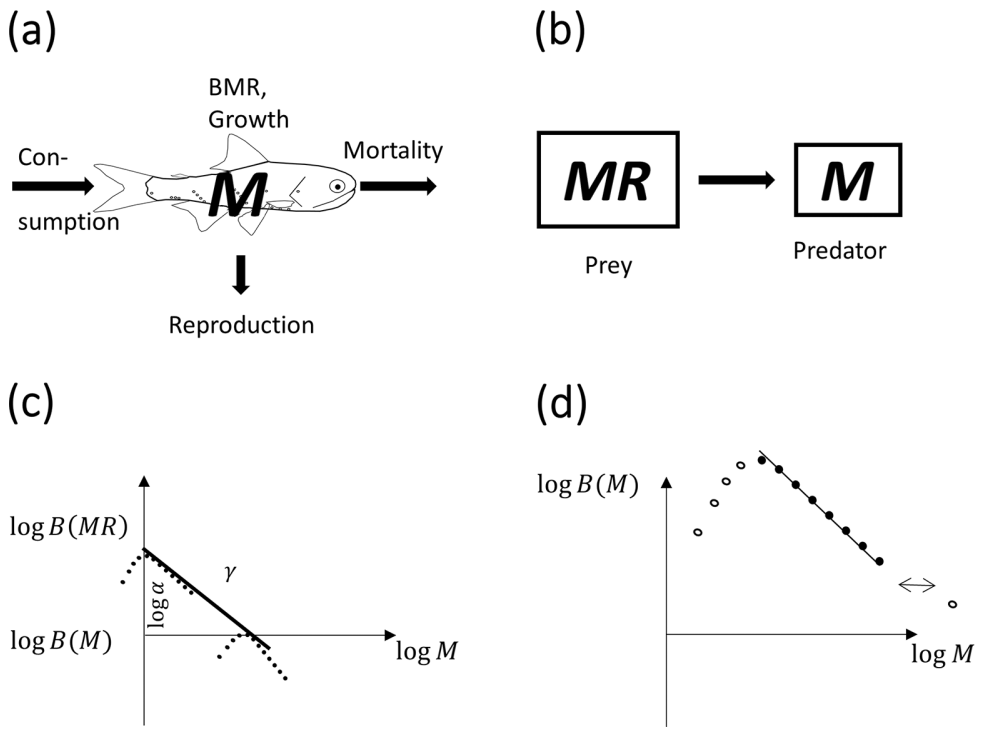

FIGURE 1 Schematic representation of size spectra models and data selection related to (a) metabolic size spectra models, (b) predator–prey models (where arrow indicates biomass flow consumed by predator of body mass, M), (c) linear model of spectral densities in the BDKT model of predator and prey each represented by dome-shaped patterns, and (d) selection of data by ecosystem component for the synthetic NBSS analysis (selected, solid circles; unselected, open circles), where the double-sided arrow indicates a gap with zeroes. BMR, basic metabolic rate; $B(M)$ and $B(MR)$, spectral densities of predator and prey; M, body mass of predator; R, prey–predator mass ratio, that is, the inverse of PPMR; or in (d) as $B(M)$ referring to generic spectral density. Illustration credit: H. O. Fock.

function (Arim et al., 2011; Brown et al., 2004). In cases where predation is not so significant and/or transfer efficiency is high, NBSS slopes are predicted to range between −0.75 and −1.

In this study, we analyzed community size spectra composed of phytoplankton, meso- and macrozooplankton, and total micronekton (including mesopelagic fishes) across seven regions of the Atlantic, ranging from 30° N to 35° S with different levels of nutrient supply and coastal affiliation. By integrating components sampled with different methodologies and time frames, we assembled spectra of ecosystem components into "synthetic spectra" that are supposed to resemble the genuine synoptic spectra representative of distinct oceanographic settings and productivity regimes. At the regional level, NBSS analyses have previously been carried out only for specific ecosystem components, for example, for zooplankton in the northern Canary Current Upwelling System (nCCUS) (Couret et al., 2023) and NE Brazilian shelf and oceanic islands (de Figueiredo et al., 2025; Lira et al., 2024), and for mesopelagic fishes in the equatorial (EQU) region and the Benguela Upwelling System (BUS) (Fock et al., 2025; Fock & Czudaj, 2019). At the basin scale, analyses in the Atlantic were carried out for zooplankton observed with underwater vision profiler (UVP) (Kiko et al., 2022; Soviadan et al., 2024) and water bottle-sampled phytoplankton (González-García et al., 2023; Moreno-Ostos et al., 2015). In contrast to lake ecosystems (Mehner et al., 2018; e.g., Yurista et al., 2014), synthetic analyses in the marine realm combining two or more ecosystem components are scarce and mostly focus on plankton components (Martin et al., 2006; Quinones et al., 2003; Lombard et al., 2024; Stukel et al., 2024). The inclusion of mesopelagic fishes and micronekton as such and on this scale is unprecedented except for the global modeling approach of Hatton et al. (2021).

Combining across ecosystem components and averaging across samples are essential to generate synthetic size spectra for larger bodies of water (Zhou & Huntley, 1997; see Sheldon et al., 1972). This implies that samples are combined across significant spatial and temporal scales and across ecosystem components sampled with various methodologies. Vertically, this integrates everything from the small mucus layers around phytoplankton cells with associated bacterial populations, that is, "phycospheres" (Azam & Malfatti, 2007), of which billions are contained in a single water bottle sample, to microlayers comprising strong environmental gradients such as deep chlorophyll maxima with associated changes in the size structure of the phytoplankton (Álvarez et al., 2008) to macrolayers such as acoustic deep and surface scattering layers of dense micronekton (Czudaj et al., 2021; Hoving et al., 2020; Marohn et al., 2021). However, this vertical structure is effectively redistributed by means of two processes, that is, diel vertical migration (DVM) and particle sinking. DVM in particular for metazooplankton can change and modify phyto- and zooplankton food web and size structure at smaller scales (Cornils et al., 2022; Kang et al., 2023). Sinking as the second process generates a vertical connectivity given that organic particles and aggregates act as vehicles to transport their microbial communities from the surface into deeper waters (Iversen, 2023). Horizontally, regional oceanography generates coherent water bodies that can be applied as proxy to understand biological processes leading to the delineation of biogeographical provinces in the sea, sharing common attributes in terms of species composition and productivity regime (Longhurst, 2007; Platt & Sathyendranath, 1999; Sutton et al., 2017). Temporally, observations with inherent intra- and interannual variability are combined. In the tropical and subtropical Atlantic, intra-annual variability exceeds interannual variability by a factor of 2–5 (Picaut et al., 1984). However, despite high intra-annual variability, regional differences can be maintained if the underlying water mass distributions are respected. Fock et al. (2025) analyzed micronekton size spectra from two seasons in two regions of the BUS governed by specific water masses. They stated that NBSS slopes differed seasonally but were on average steeper in the more nutrient-enriched region. Likewise, biomass on average was higher, indicated through the intercept of the linear NBSS model.

We ask whether synthetic NBSS parameters consistently describe the regional community structure as a function of the underlying productivity regime and oceanography. This assumes vertical and horizontal coherence of water bodies and communities. Secondly, productivity can be expected to consistently impact NBSS parameters of the phytoplankton–zooplankton–micronekton system in four ways, that is, (1) by determining the degree of dominance of heterotrophic zooplankton over phytoplankton; (2) by determining the average level of biomass or elevation of NBSS; (3) by steepening the slopes in eutrophic regions; and (4) by considering the specific role of gelatinous, that is, volume-rich, organisms in inverted, top-heavy plankton food webs (Lombard et al., 2024).

The following objectives were addressed by applying two biomass units in this study, carbon contents and biovolume. Size spectra are analyzed in their linearized form, that is, as a log–log model:

1. Firstly, calculate the size spectrum slope to investigate whether biovolume-based size spectra are more top-heavy than carbon-based size spectra.

2. Secondly, analyze differences in community structure by means of standardized spectral densities of heterotrophic ecosystem components, in particular zooplankton in relation to each other and to autotrophic, that is, phytoplankton biomass. For the latter, these contrasts should be negatively correlated with primary production.
3. Thirdly, in line with the interpretation of NBSS models in relation to primary production, the regional mean spectral densities should be positively and slopes negatively correlated to primary production.

MATERIALS AND METHODS

Ecosystem components and sample selection

For carbon biomass, 379 samples were selected from seven regions based on data availability and oceanographic properties (Table 1; for regions see Appendix S1). Respectively, 536 samples were selected for biovolume, including additional records for underwater vision profiler (UVP) organic particle density combining both

TABLE 1 Available records for the synthetic normalized biomass size spectra (NBSS) analysis, based on carbon biomass.

Region	Gear	minDepth (m)	maxDepth (m)	No. records included	Years covered	Months covered
BRZ_oc_isl	Bongo	0	200	9	2015	10
BRZ_oc_isl	Niskin Bottles	2	199	38	2017	4–5
BRZ_oc_isl	UVP	1	4707	10	2014–2016	5, 10
BRZ_oc_isl	Trawl meso	58	525	12	2015	10
BRZ_oc_isl	Trawl micro	60	800	4	2015, 2017	4, 10
BRZshlf	Bongo	0	200	5	2015	10
BRZshlf	Niskin Bottles	16	122	12	2017	4
BRZshlf	UVP	1	689	7	2014–2016	5, 9
BRZshlf	Trawl meso	12	500	11	2015, 2016	10
BRZshlf	Trawl micro	60	680	8	2017	4
EQU	Multinet	0	1000	20	2019	10
EQU	Niskin Bottles	5	100	32	1995–2022	1, 12
EQU	UVP	1	4700	33	2014–2016	4, 9
EQU	Trawl Aalnetz	78	680	15	2015	3–4
NBUS	Multinet	0	200	8	2019	3
NBUS	Niskin Bottles	2	20	7	2000	10
NBUS	RMT	0	602	17	2019, 2021	3, 10
NBUS	UVP	1	3515	3	2016	11
OMZ_sCCUS	Niskin Bottles	7	60	4	1996–1997	5
OMZ_sCCUS	RMT	0	670	4	2016	8
OMZ_sCCUS	UVP	1	5232	14	2013–2016	3, 9
OMZ_sCCUS	Trawl Aalnetz	76	441	9	2015	3
SBUS	Multinet	0	300	5	2019	2–3
SBUS	Niskin Bottles	56	64	2	2011	2
SBUS	RMT	0	505	13	2019, 2021	2, 9
SBUS	UVP	1	1258	4	2010	7–9
nCCUS	Niskin Bottles	5	110	28	1995–2022	5, 12
nCCUS	UVP	1	3657	27	2012–2016	3, 12
nCCUS	WP-2	0	200	6	2018–2019	2, 10
nCCUS	Trawl Aalnetz	79	623	12	2015	4

Note: Region abbreviations: BRZ_oc_isl, NE Brazil oceanic island habitat; BRZshlf, NE Brazilian shelf habitat; EQU, equatorial region; NBUS, northern Benguela Upwelling System; maxDepth, deepest depth sampled, in m; minDepth, shallowest depth sampled; nCCUS, northern Canary Current Upwelling System; OMZ_sCCUS, southern Canary Current Upwelling System oxygen minimum zone; SBUS, southern Benguela Upwelling System.

zooplankton and detritus (uvpZPLD). Except for phytoplankton samples that were collected between 1995 and 2022, all other samples were collected in the period 2010–2021. The analysis of Atlantic Meridional Transect samples for phyto- and zooplankton from San Martin et al. (2006) was not duplicated.

Ecosystem components were defined by their sampling gears. Phytoplankton samples were collected from water that was collected using Niskin Bottles; WP-2 net, Multinet, and Bongo net represent zooplankton net samples; and four trawl types were deployed for micronekton and mesopelagic fishes (Rectangular Midwater Trawl RMT, trawl "Aalnetz," trawl "Meso," trawl "Micro"). See Appendix S2 for details. To account for sampling and processing biases, conversions were applied (see the next section). Net-based methods tend to undersample abundances due to net avoidance or destruction of fragile specimens, whereas in situ methods like the UVP for zooplankton and detritus and hydroacoustics for mesopelagic fishes overcome these shortcomings. For methodological details, see Appendix S2.

The Fernando de Noronha Archipelago (FNA), located in the Western Tropical Atlantic (3° 50′24″ S and 32° 24′48″ W; Figure 2), was defined as the NE Brazil oceanic island habitat (BRZ_oc_isl). Physical oceanography is determined by the central branch of the South Equatorial Current and seasonal fluctuations of the Intertropical Convergence Zone (da Silva et al., 2021; Lira et al., 2024). The NE Brazilian shelf habitat (BRZ_shlf) is influenced by the northward-flowing North Brazil Undercurrent (NBUC) that originates from the bifurcation of the southern South Equatorial Current (Dossa et al., 2021; Tosetto et al., 2021) and represents a very oligotrophic habitat.

For the open-ocean regions, the biogeographical taxonomy of Sutton et al. (2017) and Longhurst (2007) was applied (Martin et al., 2006). The EQU region is characterized by a relatively homogeneous composition of mesopelagic fishes and cephalopods due to interactions between the Equatorial Current and the Equatorial Countercurrent (see Czudaj et al., 2021; Olivar et al., 2017, fig. 12; Spalding et al., 2012). It corresponds to the

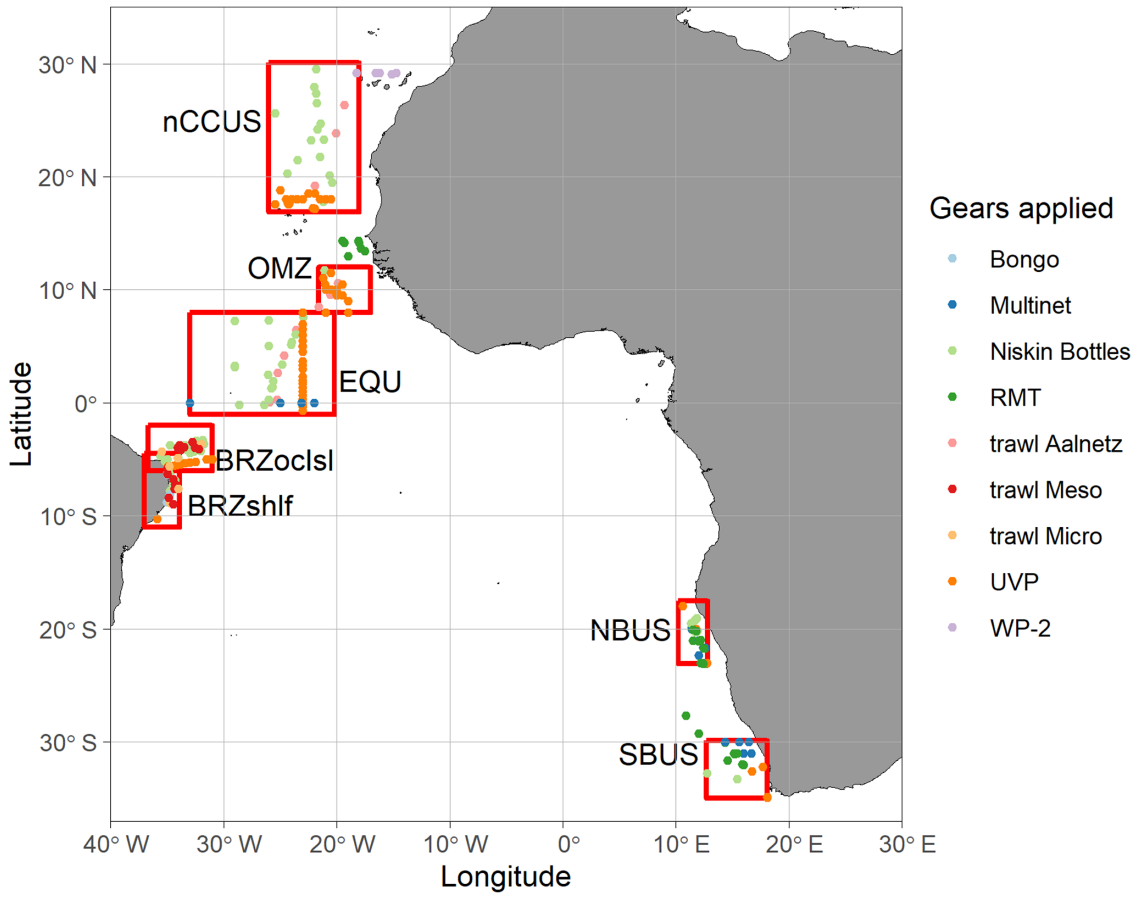

FIGURE 2 Study regions and sample distribution. BRZ_oc_isl, NE Brazil oceanic islands; BRZ_shlf, NE Brazil continental shelf, depth <800 m; EQU, northern equatorial region; NBUS, northern Benguela Upwelling System; nCCUS, northern Canary Current Upwelling System; OMZ, southern Canary Current Upwelling System oxygen minimum zone; SBUS, southern Benguela Upwelling System. Map credit: Vihtakari (2024).

northern limit of the Tropical and West Equatorial Atlantic province in Sutton et al. (2017).

The nCCUS represents the water body of the North Atlantic subtropical gyre well defined as north of the Cabo Verde Frontal Zone and separated from the coastal upwelling (Central North Atlantic in Sutton et al. (2017) and Couret et al. (2023)). The area representative of the southern Canary Current Upwelling System oxygen minimum zone (short: OMZ, else: OMZ_sCCUS) of the central eastern Atlantic lies south of the Cabo Verde Frontal system in the southern limb of the Canary Current Upwelling System and also outside the coastal zone. Its main features are low midwater oxygen concentrations and it hosts the Guinea dome, a tropical cyclonic gyre (Longhurst, 2007; Stramma et al., 2008).

The BUS is separated into a northern (NBUS) and a southern (SBUS) part by the Lüderitz permanent upwelling cell at 26° S. The northern limit is defined by the Angola–Benguela front at 19° S, and the southern limit at 34° S. The NBUS and SBUS are influenced by distinct water masses. The SBUS is dominated by nutrient-poor Eastern South Atlantic Central Water (ESACW). In the NBUS, ESACW prevails on the shelf during the main upwelling season in austral winter and spring, while nutrient-rich South Atlantic Central Water (SACW) is transported to the NBUS during the austral summer. Additional leakage from the Agulhas Current leads to entrainment of Indian Ocean water especially in the SBUS, while tropical water penetrates through the Angola–Benguela front (Duncan et al., 2022).

In some cases, regional data inventories were complemented by data from outside the chosen geographic boxes, that is, zooplankton WP-2 data in nCCUS were included, along with additional RMT data in OMZ and SBUS (see Figure 2). Data were not spread evenly inside the geographical boxes; for instance, UVP data were concentrated in the southern part of the nCCUS, and zooplankton Multinet samples were collected along the equator in EQU. Sampling was conducted either in terms of cross-sections and transects or with high regional resolution, which was in particular good for those areas for which specific multidisciplinary surveys were designed, that is, TRAFFIC campaigns in the BUS (NBUS, SBUS; see Martin et al., 2024) and ABRAÇOS cruises for the Brazilian coast habitats BRZ_shlf, BRZ_oc_isl (Bertrand, 2015, 2017; Eduardo et al., 2022).

Conversions

Sintering information across ecosystem components requires standardization of measurements with regard to measured units and protocols to account for known sampling biases (Giacomini et al., 2023). Since no comparative sampling was carried out, literature data were applied to establish conversion factors (Appendix S3).

Four types of conversions were carried out.

Tissue composition

Conversion coefficients were applied to account for taxon-specific differences in tissue composition, including preservation effects (Appendix S3: Section S1). Data from this processing stage for both biovolume and carbon biomass were available, containing micronekton without subsequent conversions (see below), that is, the unconverted "micronekton as is" (Fock et al., 2024).

Trawl type conversion (T)

While phytoplankton and UVP-measured zooplankton and detritus were all analyzed with a consistent methodology and instrumentation, net zooplankton and mesopelagic fishes and micronekton were sampled with various gears of different sizes and designs. For net zooplankton, no conversion was applied. For mesopelagic fishes and total micronekton, the conversion protocol is described in Appendix S3: Section S2.

Volumetric–gravimetric conversion (VG)

A principal difference must be considered for those taxa for which weight was determined basically as volume by image analysis (zooplankton with ellipsoidal volume models both net and UVP) and those taxa for which weight was determined gravimetrically and converted back to biovolume, of which the latter applies to biovolume calculations of micronekton and mesopelagic fishes. Conversions were carried out for micronekton and mesopelagic fishes (Appendix S3: Section S3).

Acoustic–trawl conversion (A)

Hydroacoustic biomass estimates of pelagic fishes are much higher than trawl-based estimates (Fock & Ehrich, 2010). No hydroacoustic data were evaluated for this study but in previous investigations where fish were included, hydroacoustic data have been applied (Giacomini et al., 2023; Hatton et al., 2021; Yurista et al., 2014). Hence, a conversion factor was applied for mesopelagic fishes and total micronekton to account for the methodological difference (Appendix S3: Section S4).

Starting with unconverted micronekton, termed "micronekton as is," T, VG, and A conversions were subsequently included in the analysis as indicated.

Data preparation and size spectra calculation

Typology of size spectrum models

In marine systems, three classes of size spectrum models have been applied, although the range of size spectrum and allometric models is much broader (Andersen et al., 2009, 2016; Martens et al., 2015; Yvon-Durocher et al., 2011). In all cases, the size spectrum models can be expanded from groups of organisms with similar characteristics and functions to the community level (Stemmann & Boss, 2012).

The first model category focuses on metabolism, that is, basal metabolic rate (BMR), growth, feeding, and mortality relationships, which can be described in terms of allometric functions of body size M (Figure 1a). Metabolism can be scaled differently, either to surface area with a predicted scaling of 2/3 or in the form of resource transport networks with a predicted scaling of 3/4, that is, Kleiber's law (Glazier, 2014). Platt and Denman (1977) and Silvert & Platt (1978, hereafter PDS) described NBSS as

$$B(M) \propto M^{-(1-x+\alpha\Lambda+q)}, \quad (1)$$

where x is the exponent of the turnover or loss function including predation, with a nominal value of 0.28. The dimensionless product $\alpha\Lambda$ is comprised of the scaling factors for the turnover loss term and the term of metabolism with a value in the range of 0.1–0.5. The term q is the scaling factor for losses to the decomposer food chain. Taking into account that two main processes with opposing signs take place in the microbial loop, that is, microbial turnover as opposed to subsequent heterotrophic incorporation, q is suggested to be ~0 (Silvert & Platt, 1978). The MTE (Arim et al., 2011; Brown et al., 2004; Brown & Gillooly, 2003) builds on the 3/4--scaling law (which is questioned for some ecosystem components; Hatton et al., 2021; Huete-Ortega et al., 2011; Marañón et al., 2007). Energy allocation E should be the same across the body mass range considered (energy equivalence rule; Allen et al., 2002), thus scaling biomass B as M^0 between TLs and subsequently with B as $M^{0.25}$ within a TL where no predation takes place (Jennings & Mackinson, 2003). MTE describes the NBSS for biomass, scaled as

$$B(M) \propto aM^{\gamma} = aM^{\frac{\log 10(\mathrm{TTE})}{\log 10(\mathrm{PPMR})} - 0.75}. \quad (2)$$

The first term of the exponent is the biomass transfer function by means of trophic transfer efficiency (TTE) and predator–prey mass ratio (PPMR) with an expected value of −0.25 which is 0 for the within-TL case. Equation (2) can be applied to calculate TTE as $\mathrm{TTE} = \mathrm{PPMR}^{\gamma+0.75}$. MTE has been applied to explain seasonal differences in temperature and productivity in micronekton assemblages of the BUS (Fock et al., 2025), interdecadal differences in mesopelagic assemblages of the tropical and subtropical Atlantic (Fock & Czudaj, 2019) and Pacific (Hunt et al., 2015) as well as North Sea demersal fishes (e.g., Jennings & Mackinson, 2003).

The second approach puts an emphasis on population dynamics, which will refer, in this study, to all organisms belonging to either phytoplankton or zooplankton, and fishes. Heath (1995) developed a model where the difference from one size class to another depends on individual growth and mortality. Zhou & Huntley (1997, herafter ZH) included intrinsic rates of growth and mortality, and their NBSS slope is eventually determined by the ratio of the intrinsic growth rate μ over the individual growth rate g:

$$B(M) \propto M^{-1+\frac{\mu}{g}}. \quad (3)$$

The sign of μ determines whether the slope is <-1 (negative sign = net mortality) or >-1 (positive sign = net increase).

A third category of models is built as predator–prey models describing the transfer of biomass between two TLs by means of a feeding term with a certain transfer efficiency KF and changes in specific production P of the prey (Figure 1b), both as a function of predator body size M so that prey size is MR accordingly (Boudreau et al., 1991; Kerr & Dickie, 2001; Thiebaux & Dickie, 1992, 1993, hereafter BDKT):

$$\frac{B(M)}{B(MR)} \propto \frac{KF}{P} = \frac{a'M^{\gamma'}}{a''M^{\gamma''}} = \frac{a'}{a''}M^{\gamma'-\gamma''} = aM^{\gamma}. \quad (4)$$

The BDKT model does not imply that the NBSS is a monotonically decreasing function, but rather is comprised of domes of biomass separated by PPMR, or its inverse R (Figure 1c).

All models have certain features in common. MTE predicts NBSS slopes of about −1 depending on transfer efficiency and PPMRs, while PDS predicts a range from −0.82 to −1.22. MTE and BDKT include the body mass

ratio between prey and predators and feeding efficiency, and ZH and PDS include mortality. In turn, MTE and ZH provide different explanations for shallower slopes >−1. MTE predicts a common slope for the entire system, whereas ZH allows for different slopes in different parts of the *M* range. None of the models includes all the processes that were indicated by Rodríguez (1994).

Rationale of the analysis

Data were sampled with great spatial, temporal, and vertical heterogeneity. Therefore, to obtain a robust regional mean for each ecosystem component, samples were averaged to compensate for small-scale patchiness. If possible, seasonal differences were eliminated by averaging across repeated cruises and differences in spatial distribution by accounting for water body affiliation and bathymetry as well as vertical averaging. Averaging across samples increases sample size, allowing for closing zero gaps in individual size spectra, since size spectrum classes with zero abundance are not defined at the log scale (Gómez-Canchong et al., 2013). In the same way, averaging is understood as a means to overcome issues of small sample sizes of UVP measurements (Soviadan et al., 2024). In line with Fock et al. (2025), the 10^{-7} ppm detection threshold of a specimen of a given size (Witek & Krajewska-Soltys, 1989) is applied to indicate unduly range extensions of size spectra in three exemplified scenarios, each for a single sample and for the average of five samples taken. In the first scenario, this refers to a 1-mg specimen of a sample size of 0.01 m^3 representative of the UVP samples, where the typical depth-integrated UVP sample size lies in the range of 0.03–0.15 m^3 (Kiko et al., 2017). Secondly, it was applied to a 1-g specimen sampled within a sample volume of about 10^5 m^3 representative of the relatively small RMT, and thirdly, to a 1-g specimen in a sample volume of about 10^7 m^3 representative of the larger "Aalnetz" and "Micro" trawls.

Of the size spectrum toolbox, BDKT allows for the analysis of PPMR and MTE to infer TTEs from size spectrum slopes with a known PPMR. Hence, these two concepts were used to analyze the synthetic size spectra with a log–log model. Following the energy equivalence rule, which states that all specimens at a certain level of body mass *M*, regardless of their role in the food web and TL, have the same requirements, MTE allows us to derive an overall NBSS slope. We consider two categories of spectra: the single synthetic spectrum for a certain region and the ensemble synthetic spectrum for all regions combined. Slopes were calculated for both single and ensemble synthetic spectra in accordance with Equation (2), and for single synthetic spectra, a further analysis of PPMR was carried out. Relationships between ecosystem components and between regions were analyzed with population marginal means models and correlated with regional primary production. Respective analyses were carried out for two units of biomass, that is, carbon contents and biovolume. With regard to uncertainty in sampling efficiency, we subsequently applied conversions for data of mesopelagic fishes and total micronekton as described above.

NBSS components

Each gear specifically samples a certain ecosystem component quantitatively within a certain size range, resulting in abundance domes as described above. For each ecosystem component, size classes from peak abundance to the last non-zero size class *M* in a consecutive order with $M_{last} > M_{peak}$ were selected (Figure 1d, selection of unbiased size classes; see Dugenne et al. (2024)). Log-binning with normalization was applied to averaged samples, analogous to the LBNbiom method (Edwards et al., 2017) already applied to mesopelagic fishes (Fock et al., 2025; Fock & Czudaj, 2019). Binning was carried out in $\log_2$-bins, that is, octave scale (Sheldon et al., 1972; William Gary Sprules & Barth, 2015) with bin size classes defined as 0.5, 1, 2, 4 g C or cubic millimetres biovolume, respectively. Slopes were tested according to Paternoster et al. (1998). Stations were only selected if the size spectrum of the respective ecosystem component had a clear peak with subsequently declining spectral densities. In one case, station 14 in the nCCUS for zooplankton biovolume, this did not apply (Figure 3).

Single synthetic spectrum

For the single synthetic spectrum, the BDKT model with constant *R* in the log–log form implies a linear relationship (Figure 1c). The ratio $1/R$ is the PPMR. This allows for two ways of analysis. Firstly, given a constant ratio of spectral densities, that is, sampling from the same assemblage, the log of the intercept should be negatively correlated to $\gamma \times \log(M)$:

$$-\log a = \log\left(\frac{B(MR)}{B(M)}\right) + \gamma \log M \quad (5)$$

This can be shown through resampling within a given assemblage where the condition $\log B(M) - \log B(MR) = \text{const.}$ applies, to indicate how sample composition affected the within-assemblage variability (Appendix S4). The negative relationship between slope and intercept is

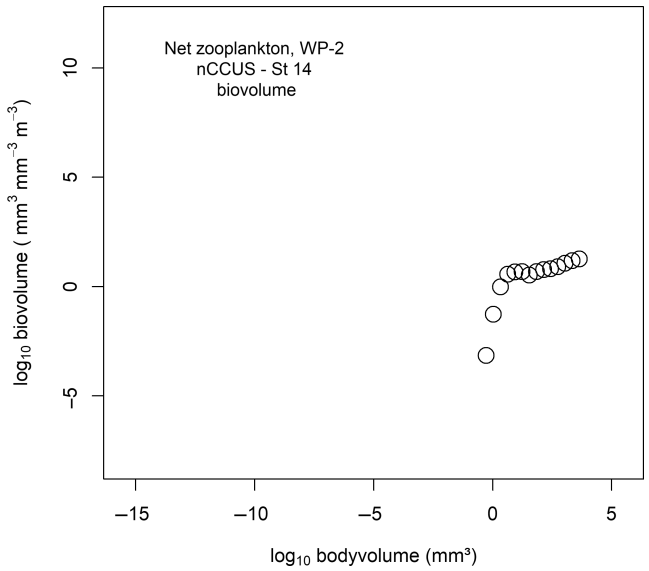

FIGURE 3 Size spectrum for zooplankton biovolume, Station 14, northern Canary Current Upwelling System (nCCUS), 2018. See Couret et al. (2023) for details of the zooplankton sampling program.

well known (Gómez-Canchong et al., 2013), and it differs depending on ecosystem type (see Moreno-Ostos et al., 2015, fig. 6). The second application is that Equation (4) can be solved as a difference equation, with the solution yielding a quadratic term plus a periodic part. The quadratic part is understood to represent the abundance dome of the respective ecosystem component (Yurista et al., 2014). Not including the periodic part, Thiebaux and Dickie (1993) and Thiebaux and Dickie (1992) showed that in the solution

$$\log B(M) = \log B_0 + 0.5c_0[\log(M) - \log(M_0)]^2, \quad (6)$$

the (x,y)-position of the apex of the abundance dome is defined by $(\log(M_0), \log(B_0))$ and c_0 describes the curvature of the parabola and is negative. Accordingly, M_{0_predator} and M_{0_prey} can be determined, and the difference between them indicates PPMR. The above approach follows a bottom-up rationale, while Rossberg et al. (2019) demonstrated that dome-shaped patterns likewise can arise from top-down trophic cascades. Regressions were carried out with the R package *nlme* (Pinheiro et al., 2021).

Ensemble synthetic spectrum

The basic form of the population marginal means model with two categorical variables is (see Searle et al., 1980, eq. 2.1)

$$\mu_{mn} = \mu + \varphi_m + \beta_n, \quad (7a)$$

where μ is a general mean and φ and β are effects without interactions. Population marginal means models calculate least squares means as within-group means appropriately adjusted for the other effects in the model, which in this case is the dependence of the mean on size class M_i.

The general mean for the MTE model in its log–log form is defined by the slope of the entire ensemble spectrum times the log of the biomass size class M, that is, γ log M_i. This ensemble mean slope has been commonly applied to describe generic size spectra properties ("system slope" [Zhou & Huntley, 1997], "global slope" [Blanco et al., 1994], and "overall regression" [Mehner et al., 2018]). Subtraction of the general mean on both sides sets the factor values in relation to the difference between the observation and the general mean. Here, factors region r_k and ecosystem component c_j are considered. Analyzing the log–log model with two factors implies that the intercept parameter a in Equation (2) would be a yet-undefined multiplicative effect. Therefore, the log–log analysis is separated into two equations, one for either factor, resulting in population marginal means either by region or by ecosystem component, but not in the interaction of region and ecosystem components. With respective error terms, we get

$$logB_{jk}(M_i) - \gamma logM_i = log\, c_j + \epsilon_j \quad (7b)$$

$$logB_{jk}(M_i) - \gamma logM_i = logr_k + \epsilon_k \quad (7c)$$

where subscripts indicate ecosystem components j and regions k, respectively. To avoid duplication within ecosystem components, the ensemble mean slope is calculated from three ecosystem components, that is, phytoplankton, one zooplankton component (either net zooplankton or UVP-measured zooplankton), and total micronekton. Since no net zooplankton was available for the OMZ region, OMZ data were not included in the calculation of the ensemble mean slope. Slopes were calculated either as a simple linear model (lm) or with a mixed-effects model (lme), where the offset is allowed to vary by region. The R system packages *base* and *lme4* were applied for regressions (Bates et al., 2015; R Development Core Team, 2023). For model evaluation, the Akaike information criterion (AIC) was applied and interpreted in terms of evidence ratio as $\exp(-0.5\Delta)$, where Δ is the difference of AIC values between two models (Burnham et al., 2011). Based on the lm-slope, region and ecosystem component effects were obtained as estimated marginal means in terms of mean expected spectral densities at a given M (Lenth, 2024; Searle et al., 1980). The differences

on a log scale, that is, contrasts (also biomass ratios, see Stukel et al., 2024), between components within and across all regions and regions across all components are thus related to log c_{kj}, log c_j, and log r_k and were calculated using the R package *emmeans* (Lenth, 2024). Multiple comparisons of region and component marginal means were carried out as *t*-test with Šidák correction (Midway et al., 2020). Differences in slopes were tested by means of type III ANOVA on the joint biovolume and carbon data set for three ecosystem components as described above with conversions and biomass unit as factors.

Environmental data

Information on mean annual primary production as climatological proxy was extracted for the center of each region from publicly available modeled data based on remote sensing (Kaschner et al., 2008).

RESULTS

Ensemble mean slopes for biovolume- and carbon-based NBSS

The ensemble mean slope is essential to build the marginal means model and tested with different combinations of data conversions and biomass units. The plot of the ensemble mean slope model for carbon contents prior to applying conversion factors to spectral densities of micronekton and mesopelagic fishes, that is, "micronekton as is," shows how sensitive the model is regarding coverage of ecosystem components included (Figure 4). For instance, the gap between phyto- and zooplankton indicates that microzooplankton data were not available. For the ecosystem components considered, the phytoplankton–net zooplankton–micronekton model (solid line, Figure 4) on average yields moderate negative residuals for the micronekton and mesopelagic fishes' components and mostly positive residuals for net and underwater vision profiler (UVP)-measured zooplankton. Selecting phytoplankton and net zooplankton alone to build the ensemble mean slope model would result in strongly negative residuals for the mesopelagic fishes and micronekton (Table 2, model 32). The resulting slope is shallower and thus indicates a top-heavier system. In turn, selecting only phytoplankton for the ensemble mean slope model would generate strongly positive residuals for the zooplankton components. It is further clear that the conversions would increase the numbers for total micronekton and mesopelagic fishes, thus reducing the gap between the two zooplankton components and

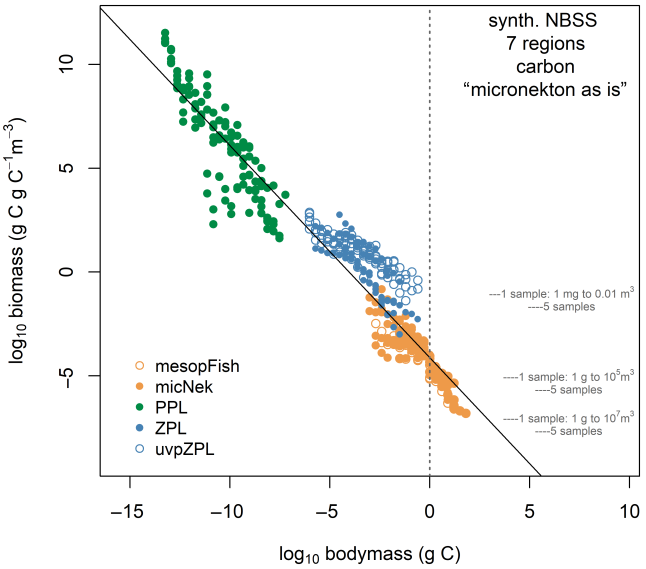

FIGURE 4 Ecosystem components selected for synthetic normalized size spectrum analysis. Regression line representing ensemble mean slope according to model 8 for three ecosystem components (solid line), depicted in Table 2. The 10^{-7} ppm detection threshold of specimens of different sizes are indicated for three different sampling scenarios each for a single sample and averaged across five samples. UVP-measured zooplankton fairly well respects the first detection limit threshold (blue circles), while sample sizes for net zooplankton are relatively larger allowing for extended spectra (blue dots). "Micronekton as is" refers to unconverted micronekton; MicNek, total micronekton; mesopFish, mesopelagic fishes; PPL, phytoplankton; uvpZPL, UVP-measured zooplankton; ZPL, net zooplankton.

the two former ecosystem components and making slopes shallower.

According to the AIC values, models 16, 24, and 28 were the best models to explain the data with an AIC < 800, all carbon-based (Table 2). The best model 28, with a slope of −0.894 incorporating all conversions, was significantly different from the third best model 16 with a slope of −0.972 (Table 2, dd). While model 16 slope was marginally different from the theoretical MTE slope of −1 ($p = 0.053$), the slope estimate for the third best biovolume model (model 15, slope = −0.943) was significantly different from −1 ($p < 0.001$), as were the best biovolume models, models 23 and 27. The evidence ratio between models 24 and 16 is 11-fold, and 270-fold between models 28 and 24. If model 16 is assumed to represent the default overall MTE slope of −1 with 10% TTE and a PPMR of 10,000:1, then the evidence of our data that the slope is > −1 is about 3000-times stronger (=11 × 270). For both biovolume and carbon biomass, the differences between best and second-best models were significant (Table 2, cc, dd).

TABLE 2 Calculation of ensemble mean slopes for six regions (excluding OMZ) with two methods and three and two ecosystem components, respectively.

Model coverage/test	Biomass unit	Ensemble mean slope	SE	AIC	*p* value of *Z* score
Three ecosystem components					
"Micronekton as is"					
(1) lm: PPL–uvpZPL–MicNek	Volume	−0.93703	0.01760	1000.4	
(2) lm: PPL–uvpZPL–MicNek	Carbon	−0.98491	0.01713	1044.4	
(a) Difference in slopes (1) and (2)					0.025
(3) lm: PPL–ZPL–MicNek	Volume	−0.97944	0.01467	883.6	
(4) lm: PPL–ZPL–MicNek	Carbon	−1.02150	0.01542	873.3	
(b) Difference in slopes (3) and (4)					0.017
(c) Difference in slopes (1) and (3)					0.032
(d) Difference in slopes (2) and (4)					0.042
(5) lme: PPL–uvpZPL–MicNek	Volume	−0.93441	0.01665	988.7	
(6) lme: PPL–uvpZPL–MicNek	Carbon	−0.98746	0.01624	1032.4	
(e) Difference in slopes (5) and (6)					0.016
(7) lme: PPL–ZPL–MicNek	Volume	−0.97470	0.01355	856.3	
(8) lme: PPL–ZPL–MicNek	Carbon	−1.01872	0.01408	846.2	
(f) Difference in slopes (7) and (8)					0.012
(g) Difference in slopes (5) and (7)					0.030
(h) Difference in slopes (6) and (8)					0.072
Micronekton T converted					
(9) lm: PPL–uvpZPL–MicNek	Volume	−0.90519	0.01648	958.0	
(10) lm: PPL–uvpZPL–MicNek	Carbon	−0.93210	0.01621	923.6	
(i) Difference in slopes (9) and (10)					0.122
(11) lm: PPL–ZPL–MicNek	Volume	−0.94620	0.01435	841.9	
(12) lm: PPL–ZPL–MicNek	Carbon	−0.97072	0.01507	801.0	
(j) Difference in slopes (11) and (12)					0.112
(k) Difference in slopes (9) and (11)					0.030
(l) Difference in slopes (10) and (12)					0.041
(13) lme: PPL–uvpZPL–MicNek	Volume	−0.90704	0.01575	952.3	
(14) lme: PPL–uvpZPL–MicNek	Carbon	−0.93756	0.01580	926.3	
(m) Difference in slopes (13) and (14)					0.086
(15) lme: PPL–ZPL–MicNek	Volume	−0.94349	0.01343	828.8	
(16) lme: PPL–ZPL–MicNek	Carbon	−0.97215	0.01438	798.5	
(n) Difference in slopes (15) and (16)					0.072
(o) Difference in slopes (13) and (15)					0.961
(p) Difference in slopes (14) and (16)					0.052
Micronekton T and VG converted					
(17) lm: PPL–uvpZPL–MicNek	Volume	−0.90332	0.01648	958.2	
(18) lm: PL–ZPL–MicNek	Volume	−0.94421	0.01441	844.2	
(19) lme: PPL–uvpZPL–MicNek	Volume	−0.90526	0.01572	951.5	
(20) lme: PPL–ZPL–MicNek	Volume	−0.94155	0.01345	829.8	
(q) Difference in slopes (17) and (10)					0.106
(r) Difference in slopes (18) and (12)					0.102

TABLE 2 (Continued)

Model coverage/test	Biomass unit	Ensemble mean slope	SE	AIC	*p* value of *Z* score
(s) Difference in slopes (19) and (14)					0.073
(t) Difference in slopes (20) and (16)					0.060
Micronekton T and VG and A converted					
(21) lm: PPL–uvpZPL–MicNek	Volume	−0.83131	0.01456	888.3	
(22) lm: PPL–uvpZPL–MicNek[a]	Carbon	−0.85734	0.01469	867.2	
(u) Difference in slopes (21) and (22)					0.104
(23) lm: PPL–ZPL–MicNek	Volume	−0.86824	0.01399	828.2	
(24) lm: PPL–ZPL–MicNek[a]	Carbon	−0.89201	0.01486	793.7	
(v) Difference in slopes (23) and (24)					0.122
(w) Difference in slopes (21) and (23)					0.033
(x) Difference in slopes (22) and (24)					0.048
(25) lme: PPL–uvpZPL–MicNek	Volume	−0.83283	0.01377	878.2	
(26) lme: PPL–uvpZPL–MicNek[a]	Carbon	−0.86282	0.01419	866.8	
(y) Difference in slopes (25) and (26)					0.064
(27) lme: PPL–ZPL–MicNek	Volume	−0.86589	0.01285	806.5	
(28) lme: PPL–ZPL–MicNek[a]	Carbon	−0.89393	0.01389	782.5	
(z) Difference in slopes (27) and (28)					0.069
(aa) Difference in slopes (25) and (27)					0.039
(bb) Difference in slopes (26) and (28)					0.058
(cc) Difference in slopes (20) and (27)					<0.001
(dd) Difference in slopes (16) and (28)					<0.001
Two ecosystem components					
(29) lm: PPL–ZPL	Volume	−0.88065	0.02144		
(30) lm: PPL–ZPL	Carbon	−0.91579	0.02382		
(31) lme: PPL–ZPL	Volume	−0.86859	0.01972		
(32) lme: PPL–ZPL	Carbon	−0.90732	0.02187		

Note: Micronekton modifications: "Micronekton as is," without conversions.

Abbreviations: *A*, conversions applied for differences regarding hydroacoustic biomass estimation; AIC, Akaike information criterion; lm, linear model without random effects; lme, linear mixed-effects model with random effects for each region; MicNek, total micronekton; PPL, phytoplankton; *T*, conversions applied for different trawl sizes; uvpZPL, UVP-measured zooplankton; VG, conversions applied for volumetric–gravimetric differences in mass determination; ZPL, zooplankton.

[a]VG conversion does not apply to carbon biomass.

Comparing synthetic NBSS based on either carbon contents or biovolume shows that the hypothesis of top-heavier size spectra if biomass is measured in biovolume units is true in pairwise comparisons if no conversions for sampling bias were undertaken for micronekton in relation to zooplankton (Table 2, a, b, e, and f). Further pairwise comparisons indicate that biovolume slopes were marginally larger than their carbon counterparts (Table 2, m, n, s, t, y, and z), or in four cases not significantly different (Table 2, i, j, u, and v), depending on combinations of conversions. In turn, ANOVA reveals significant slope effects of biomass unit ($p = 0.0005$ for the binary interaction effect slope: biomass unit) and of conversions ($p < 0.0001$ for the binary interaction effect slope: conversion type; Appendix S5). This perception remains unchanged even considering the ANOVA, a case of multiple comparisons with Bonferroni adjustments of the significance levels, either for three types of conversions ($p = 0.0015$ for the interaction effect slope: biomass unit) or for 10 different ways of conducting linear mixed-effects models (see Table 2) ($p = 0.005$ interaction effect slope: biomass unit).

In all regressions, the mixed-effects models with net zooplankton were better in terms of AIC than the models for UVP-measured zooplankton. While there was no significant difference between the best linear (Table 2, model 24) and the best mixed-effects model (Table 2, model 28) in terms of slopes ($p = 0.46$), in most cases

there was a significant difference between models for net zooplankton and those for UVP-measured zooplankton (Table 2, c, d, g, k, l, w, x, aa) as compared to marginally different (Table 2, h, p, and bb) or insignificant differences (Table 2, o). Slopes by region are shown in Appendix S6: Tables S1 and S2.

Analysis of contrasts I: Plankton spectral densities in relation to other ecosystem components

The ensemble mean slope model for carbon contents (Figure 4) shows that residuals for zooplankton were mainly positive as compared to residuals of phytoplankton, micronekton, and mesopelagic fishes. The application of converted figures for micronekton reduces the gap between zooplankton and total micronekton, which is shown in the analysis of estimated mean marginal spectral densities by ecosystem component. Because different slopes were used in the analyses for carbon biomass (Figure 5a,b,d), the marginal means differed in absolute terms. In all four analyses (Figure 5a–d), there was no significant difference of marginal means among phytoplankton (PPL), total micronekton, and mesopelagic fishes. The relative difference, that is, contrast, between T converted total micronekton considering the effect of different trawl sizes and phytoplankton was ~0. In turn, contrasts for net zooplankton in relation to total micronekton were 0.88 for T converted and 1.41 for "micronekton as is." This can be interpreted as a relatively higher spectral density of zooplankton by factors of 7.5 ($=10^{0.88}$) and 25.1, respectively, which helps understand the effect of T conversion, which on average is ~5 for the larger graded nets, and hence the combined effect is ~5 × 5 (~7.5) ≈ 25. The third conversion step, a conversion to account for the bias between hydroacoustic and trawl estimates of micronekton biomass, with a further factor of 13.9 for micronekton and mesopelagic fishes, eliminates the difference to zooplankton ZPL (Figure 5d). At this step, total micronekton and uvpZPL were significantly different from phytoplankton PPL, and the estimated marginal mean spectral densities of all heterotrophic components were higher than for phytoplankton.

Zooplankton and detritus exceeded phytoplankton significantly. The analysis of trawl size and volumetric–gravimetric converted biovolume (T + VG) indicated a contrast of 2.77 between UVP-measured organic particle density (uvpZPLD) (Figure 5c), and hence a 500-times higher concentration of non-autotrophic particles as compared to phytoplankton. Taking the uvpZPL–ZPL contrast as an indicator of a potential methodological difference between selective net sampling and nondiscriminatory UVP sampling (1.04, equivalent to "intercept adjustment"; see Lombard et al., 2024) and the UVP relative percent error and sampling bias of 35% (see Bisson et al., 2022, with log10(1) − log10(0.65) = 0.19), a minimum value of a 35-times ($=10^{2.77-1.04-0.19}$) higher concentration of non-autotrophic particles and zooplankton as compared to phytoplankton was obtained.

The contrasts uvpZPL–ZPL by carbon contents and biovolume were 0.54 (factor 3.5) and 1.04, respectively (factor 11, positive: uvpZPL > ZPL). This in turn was very close to the factor of approximately 7.1 (measured at $10^{3.3}$ µm equivalent spherical diameter [ESD]) for the global carbon contrast uvpZPL–ZPL (Soviadan et al., 2024, fig. S1).

Analysis of contrasts II: Relationships to primary production

The marginal estimates by ecosystem indicated that zooplankton on average were relatively more abundant than phytoplankton, that is, the contrasts zooplankton–phytoplankton were positive on average and vice versa. Resolving the analysis of contrasts by region and ecosystem component allowed us to correlate the trend of contrasts with primary production (Tables 3–5).

For carbon contents (Table 3), the analysis including T converted micronekton revealed two significant patterns in relation to primary production, that is, negative correlations with contrasts between total micronekton/mesopelagic fishes and net zooplankton and positive correlations with contrasts between phytoplankton and total micronekton/mesopelagic fishes. For the former, this means that the numerical gap broadened between zooplankton and total micronekton/mesopelagic fishes with increasing primary production. For the EQU region, the contrasts 0.15 and 0.20, respectively, indicated a slight numerical dominance in favor of micronekton components (total micronekton and mesopelagic fishes), while in the Benguela system this was opposite with values <−2. While there was no significant relationship for zooplankton contrasts with phytoplankton, a positive primary production relationship appeared for phytoplankton contrasts in relation to total micronekton/mesopelagic fishes. Contrasts were negative for the EQU region (−0.24 to −0.29) and the Brazilian regions (−0.96 to −1.16), that is, micronekton components were relatively more abundant than phytoplankton, while at increased trophic state phytoplankton starts to relatively increase and the contrasts level off above 550 mg C m^{-2}

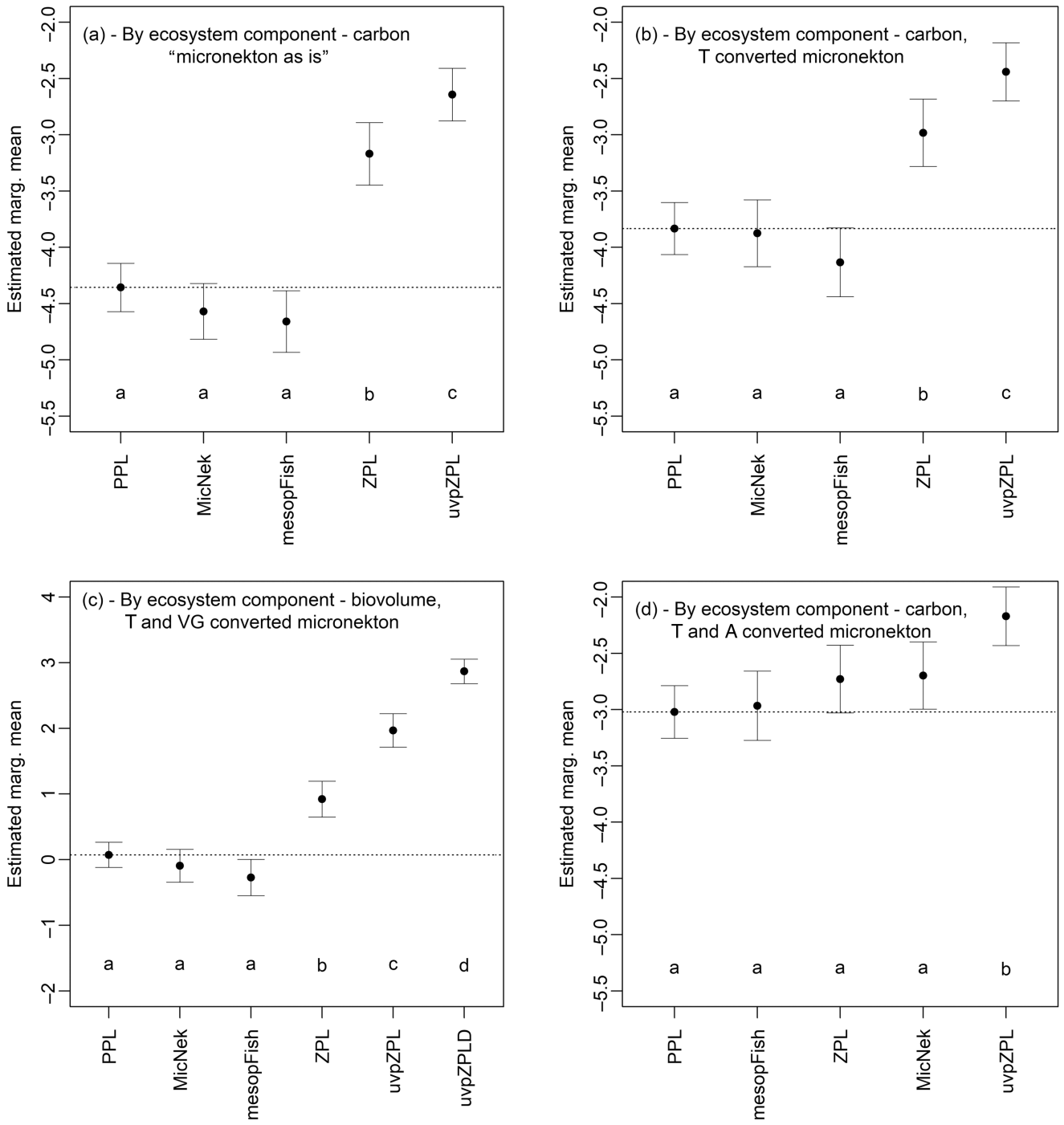

FIGURE 5 Estimated mean marginal (marg.) spectral densities by ecosystem component and by different biomass units and respective conversions for micronekton. Error bars indicate the 95% CI of the estimated marginal mean. Means sharing a letter are not significantly different (Šidák-adjusted comparisons). Model slopes refer to Table 2. (a) Model 8, (b) model 16, (c) model 20, (d) model 28. A, acoustic–trawl conversion; MicNek, total micronekton; mesopFish, mesopelagic fishes; PPL, phytoplankton; T, trawl type conversion; uvpZPL, UVP-measured zooplankton; uvpZPLD, UVP-measured zooplankton and detritus; VG, volumetric–gravimetric conversion; ZPL, net zooplankton. "Micronekton as is" refers to unconverted micronekton.

day^{-1}, reaching values of +1.03 in the SBUS and +1.25 in the OMZ_sCCUS (Figure 6a). Including hydroacoustic conversion (*A* conversion), the figure for mesopelagic fishes shifts gradually, yielding a contrast of 0.53 for SBUS and of 0.71 for OMZ_sCCUS (Figure 6c), reaching an intersection with the zero line (equal spectral densities on either side) at ca 550 mg C m^{-2} day^{-1}. This indicates that in particular, mesopelagic fishes at a higher trophic

TABLE 3 Correlations of biomass ratios between ecosystem components, that is, contrasts, and primary production.

Contrasts/variables	mesopFish–MicNek	mesopFish–uvpZPL	mesopFish–ZPL	MicNek–uvpZPL	MicNek–ZPL	PPL–mesopFish	PPL–MicNek	PPL–uvpZPL	PPL–ZPL	ZPL–uvpZPL
mesopFish–uvpZPL	0.63									
mesopFish–ZPL	0.91*	0.83*								
MicNek–uvpZPL	0.3	0.93**	0.75							
MicNek–ZPL	0.88*	0.83*	0.99***	0.76						
PPL–mesopFish	−0.76*	−0.81*	−0.79	−0.64	−0.78					
PPL–MicNek	−0.62	−0.79*	−0.73	−0.68	−0.72	0.98***				
PPL–uvpZPL	−0.57	−0.24	−0.3	−0.03	−0.28	0.76*	0.75			
PPL–ZPL	0.35	0.16	0.45	0.1	0.45	0.2	0.29	0.53		
ZPL–uvpZPL	−0.72	−0.29	−0.77	−0.15	−0.76	0.44	0.37	0.38	−0.58	
PPclim	−0.51	−0.75	−0.91*	−0.69	−0.89*	0.76*	0.77*	0.43	−0.19	0.66

Note: Applies to micronekton converted for different trawl sizes (T converted), carbon biomass. Significance levels: $p < 0.05$ (*), $p < 0.01$ (**), and $p < 0.001$ (***).
Abbreviations: MicNek, total micronekton; PPClim, primary production in milligrams of carbon per meter squared per day; PPL, phytoplankton; uvpZPL, UVP-measured zooplankton; ZPL, zooplankton.

TABLE 4 Correlations of biomass ratios between ecosystem components, that is, contrasts, and primary production.

Contrasts/variables	mesopFish–MicNek	mesopFish–uvpZPL	mesopFish–ZPL	MicNek–uvpZPL	MicNek–ZPL	PPL–mesopFish	PPL–MicNek	PPL–uvpZPL	PPL–ZPL	ZPL–uvpZPL
mesopFish–uvpZPL	0.94**									
mesopFish–ZPL	0.57	0.55								
MicNek–uvpZPL	−0.84*	−0.61	−0.46							
MicNek–ZPL	0.03	0.05	0.84*	0						
PPL–mesopFish	−0.82*	−0.88**	−0.6	0.51	−0.17					
PPL–MicNek	−0.49	−0.63	−0.5	0.14	−0.25	0.90**				
PPL–uvpZPL	−0.69	−0.75	−0.58	0.42	−0.22	0.97***	0.96***			
PPL–ZPL	−0.37	−0.45	0.37	0.14	0.7	0.52	0.52	0.51		
ZPL–uvpZPL	−0.25	−0.21	−0.93**	0.27	−0.96**	0.31	0.29	0.34	−0.63	
PPclim	−0.65	−0.6	−0.33	0.57	0.03	0.82*	0.76*	0.86*	0.61	0.13

Note: Applies to micronekton T and VG converted, biomass in terms of biovolume. Significance levels: $p < 0.05$ (*), $p < 0.01$ (**), and $p < 0.001$ (***).
Abbreviations: MicNek, total micronekton; PPL, phytoplankton; T, trawl type conversion; uvpZPL, UVP-measured zooplankton; VG, volumetric–gravimetric conversion; ZPL, zooplankton.

TABLE 5 Correlations of biomass ratios between ecosystems components, that is contrasts, for detritus and primary production.

Contrasts/variables	mesopFish–uvpZPLD	MicNek–uvpZPLD	PPL–uvpZPLD	uvpZPL–uvpZPLD	ZPL–uvpZPLD
MicNek–uvpZPLD	−0.12				
PPL–uvpZPLD	−0.78*	0.21			
uvpZPL–uvpZPLD	0.52	0.59	−0.29		
ZPL–uvpZPLD	−0.13	0.26	0.27	0.06	
PPclim	−0.76*	0.09	0.79*	−0.66	0

Note: Applies to micronekton T and VG converted, biomass in terms of biovolume. Significance levels: $p < 0.05$ (*), $p < 0.01$ (**), and $p < 0.001$ (***).
Abbreviations: MicNek, total micronekton; PPClim, primary production in milligrams of carbon per meter squared per day; PPL, phytoplankton; T, trawl type conversion; uvpZPL, UVP-measured zooplankton; uvpZPLD, UVP-measured zooplankton and detritus; VG, volumetric–gravimetric conversion; ZPL, zooplankton.

state become numerically inferior as compared to zooplankton and phytoplankton. Accordingly, the micNek/mesopFish–ZPL contrasts are negatively correlated with PPL–mesopFish/micNek contrasts (note: one data point missing for OMZ_sCCUS due to missing ZPL in this region; Table 3).

For biovolume (Table 4), the significant correlations for PPL–mesopFish/micNek contrasts to primary production persisted, while the micNek/mesopFish–ZPL contrasts were not significantly correlated with primary production. The significant correlation for the PPL–uvpZPL contrast with primary production was further reflected in the significant PPL–uvpZPL/PPL–mesopFish/micNek correlations. For the PPL–uvpZPL contrast, the values increased from −3.5 for the Brazilian oceanic islands to −1.6 for SBUS (Figure 6b). Again, the contrasts leveled off at higher productivity levels of about 1000 mg C m^{-2} day^{-1}. This contrast correlation is in agreement with Gasol et al.'s hypothesis that heterotrophic biomass relatively increases at lower levels of primary production.

For uvpZPLD, the PPL–uvpZPLD contrast was positively correlated with primary production, that is, values range from −4.3 to −4.0 for the Brazilian regions to −2.7 for the SBUS, which reflected the primary production correlation of the PPL–uvpZPL contrast discussed above (Table 5).

Regional spectral densities and slopes in relation to primary production

Marginal means from the respective ensemble mean slopes' models were calculated for carbon biomass with T and T + A converted micronekton (Figure 7a,c) and for biovolume with T + VG and T + VG + A converted micronekton (Figure 7b,d). Generally, a positive relationship to primary production was expected, which was evident in the models for carbon contents, that is, in the version with "micronekton as is" with a significance level of $p = 0.02$ (not shown) and in the version with T and T + A converted micronekton with corresponding significance levels of $p = 0.04$ and $p = 0.01$, respectively. For the biovolume models, no significant relationship appeared. In particular, biovolume in the oceanic regions EQU, OMZ, and nCCUS increased considerably in relation to NBUS as compared to respective carbon biomass figures. Thus, the increase in biovolume relative to carbon, a supposed "jellification" effect, liquidated the strong link to primary production. In terms of NBSS slopes, a predicted negative relationship to primary production only was significant for biovolume when considering NBUS as the outlier and removing the data from the regression ($p = 0.02$; Appendix S6: Section S2).

Trophic transfer efficiency

Analyzing PPMRs according to Equation (6) furthermore allows an interpretation of the effect of switching from carbon biomass to biovolume (Table 6). Since two dome-shaped patterns are required, in cases with only one dome-shaped pattern, no results are provided (no dome present, n.d.p.; Table 6). Major differences appeared with respect to ZPL and uvpZPL values, in relation to carbon biomass and biovolume PPMR, as well as in relation to habitat. For the latter, the median PPMR for oceanic habitats was 5900:1 as compared to 437:1 for coastal and island habitats. For the trophic link of ZPL to mesopFish, the median carbon-based PPMR for matching pairs was 608:1, while for carbon biomass, the respective value was 299:1 for biovolume. For uvpZPL in relation to mesopelagic fishes, the carbon-based median was 306:1 as compared to 263:1 for biovolume. In relation to total micronekton, median figures are 80:1 for carbon biomass and 2:1 for biovolume. However, total micronekton included all gelatinous taxa so this probably was not a true PPMR. The values indicate that median PPMR was <10,000:1 in the habitats investigated, although the absolute range was between >900,000:1 and <10:1. Based on the ensemble mean slopes of models 27 and 28 (Table 2) and median PPMRs, carbon-based TTE ranged from 28.9% for open-ocean habitats to 41.9% for coastal/island habitats for the two ecosystem components considered. The respective biovolume TTE ranged from 36.8% to 49.7%.

DISCUSSION

Is there a common synthetic NBSS slope?

We calculated a common slope in terms of an ensemble mean slope, dependent on all ecosystem components and regions selected. Combining samples across ecosystem components and space was essential to derive synthetic NBSS by region, and combining the regional synthetic NBSS allowed for the calculation of an ensemble mean slope (Figure 4; see also Mehner et al., 2018). This approach allows direct comparison with existing theory, which differentiates within-TL from between-TL slopes, considering slopes built by consecutively assembling NBSS with one, two, and three ecosystem components (Brown et al., 2004; Kerr & Dickie, 2001).

Within TL: Single ecosystem components

Overall, energy flow within an ecosystem component, E, as the product of abundance scaling as $M^{-0.75}$ (equivalent

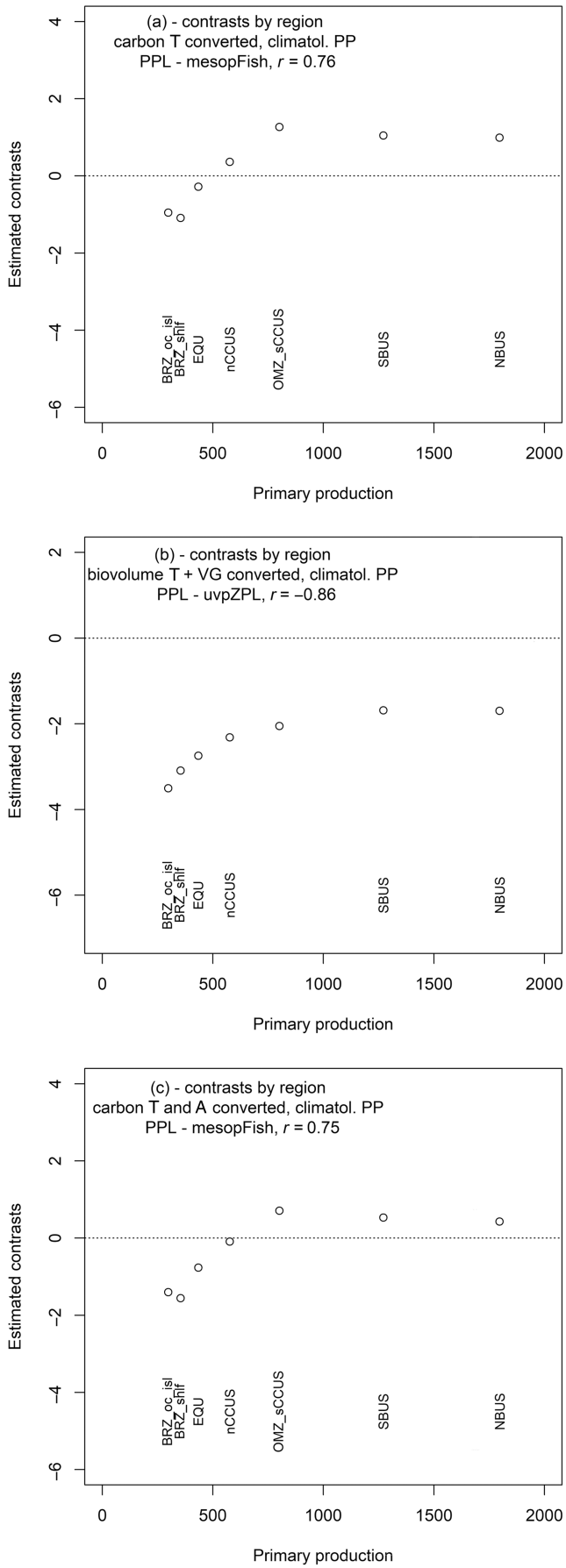

to normalized biomass $B(M)$ without turnover term, see Equation 2) and individual metabolic rate with $M^{0.75}$ should scale as M^0 (Allen et al., 2002). However, ensemble mean slopes by ecosystem component differed from −0.75 (Table 7), with much steeper slopes for phytoplankton and total micronekton than for zooplankton. The phytoplankton metabolic rate of photosynthesis of oceanic plankton does not follow the MTE scaling of $M^{0.75}$, but is higher (exponent 0.88; Padfield et al., 2018) to almost isometric (Huete-Ortega et al., 2011; exponent 1, Marañón et al., 2007). With realized NBSS slopes of approximately −1.25 for this ecosystem component (Table 7), energy flow scales as $E \propto M^1 \times M^{-1.25} \approx M^{-0.25}$, indicative of a relatively reduced photosynthesis contribution by larger cells and a superior ability of small cells to cope with oligotrophic conditions (Huete-Ortega et al., 2011; Marañón et al., 2007). Phytoplankton abundance under nutrient limitation should further scale as $M^{-2/3}$ and under light limitation as $M^{-1/3}$ (Andersen et al., 2016), leading to NBSS slopes <−1 in oligotrophic regions. Accordingly, Atlantic phytoplankton NBSS slopes shift from a minimum of −1.85 under oligotrophic conditions to values >−1.0 under higher nutrient supply (González-García et al., 2023). On the other hand, for micronekton and in particular mesopelagic fishes with visual predation in oligotrophic waters, visual detection should provide further scaling as $M^{-5/12}$ (Andersen et al., 2016), steepening the NBSS slopes towards <−1. The interpretation is the same as for phytoplankton, that is, in oligotrophic environments energy flow in mesopelagic fishes is negatively scaled to body mass and smaller specimens should be more energy efficient. Thus, under certain conditions, multiplicative scaling from processes that otherwise are not limiting may become necessary to explain

FIGURE 6 Biomass ratios between ecosystems components on $\log_{10}$-scale, that is contrasts, between (a, c) phytoplankton and mesopelagic fishes for carbon biomass with different conversions and (b) phytoplankton and UVP-measured zooplankton for biovolume in relation to primary production. A, acoustic–trawl conversion; BRZ_oc_isl, NE Brazil oceanic islands; BRZ_shlf, NE Brazil continental shelf, depth <800 m; climatol. PP, primary production as climatological mean in milligrams of carbon per meter squared per day; EQU, northern equatorial region; NBUS, northern Benguela Upwelling System; nCCUS, northern Canary Current Upwelling System; OMZ_sCCUS, southern Canary Current Upwelling System oxygen minimum zone; SBUS, southern Benguela Upwelling System; T, trawl type conversion; uvpZPL, UVP-measured zooplankton; VG, volumetric–gravimetric conversion.

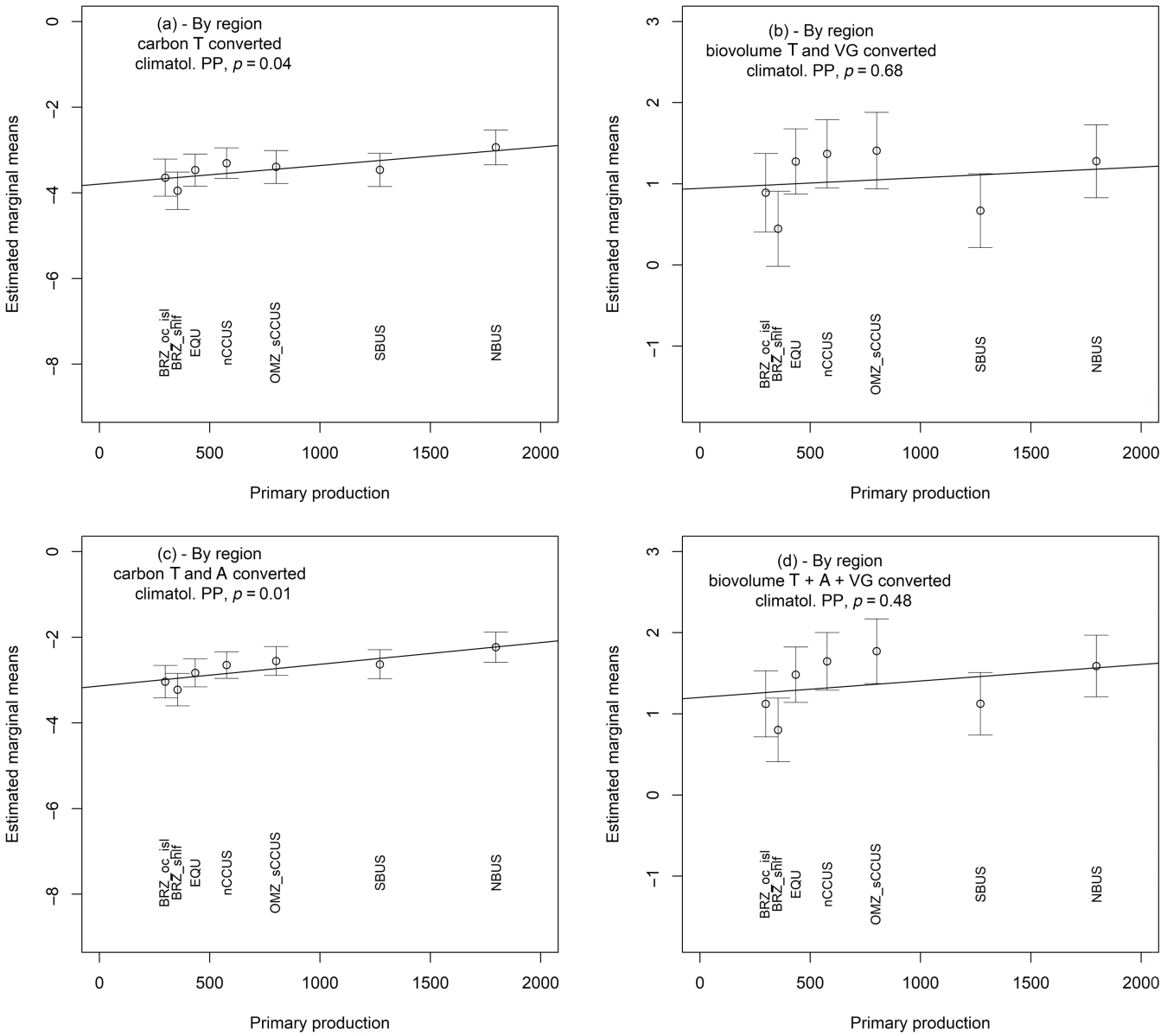

FIGURE 7 Estimated mean marginal spectral densities by region in relation to primary production for different conversions of micronekton, (a, c) for carbon biomass, (b, d) for biovolume. Error bars indicate the 95% CI of the estimated marginal mean. Climatol. PP, primary production as climatological mean in milligrams of carbon per meter squared per day. For region abbreviations, see Figure 6.

metabolism–size relationships in natural communities, leading to the framework concept of allometric scaling models to complement MTE as shown in Yvon-Durocher et al. (2011).

Between TLs: Two ecosystem components

The ensemble mean slope depended on the selection of ecosystem components included in the analysis as well as the way sampling was carried out (Figure 4). Therefore, differences in sampling regimes of different studies are supposed to have an effect on observed slopes. For the two ecosystem components considered, the PPL–ZPL ensemble mean slope in this study was >-1, that is, -0.91 for carbon biomass and -0.87 for biovolume (Figure 4, Table 7). Likewise, Lombard et al. (2024) showed that for the phytoplankton and zooplankton components (bacterioplankton only included in their daytime samples) in the tropical and subtropical Atlantic as well as globally NBSS slopes by biovolume ranged from -0.80 to -0.90 (larger than -0.9 means "top-heavy" by their definition). In their study, micronekton and mesopelagic fishes were not included, but sampling was carried out down to 500-m depth, similar to this study. Quinones et al. (2003) investigated the oligotrophic

TABLE 6 Predator–prey mass ratios (PPMRs) of mesopelagic fishes and micronekton in relation to either net zooplankton (ZPL) or UVP-measured zooplankton (uvpZPL), based on either carbon biomass (C-based) or biovolume (Vol-based) of both ecosystem components.

Region	Predator component	C-based PPMR for prey component ZPL	C-based PPMR for prey component uvpZPL	Vol-based PPMR for prey component ZPL	Vol-based PPMR for prey component uvpZPL
EQU	mesopFish	6729	n.d.p.	31,622	4645
NBUS	mesopFish	641	306	205	263
SBUS	mesopFish	481	173	109	39
OMZ_sCCUS	mesopFish	NA	1387	n.d.p.	2951
nCCUS	mesopFish	12,036	927,897	7	n.d.p.
BRZ Oc Isl	mesopFish	376	n.d.p.	394	n.d.p.
BRZ shlf	mesopFish	576	n.d.p.	498	n.d.p.
NBUS	MicNek		66		45
SBUS	MicNek		815		2
OMZ_sCCUS	MicNek		80		~0

Note: Calculated from the entire spectrum, not the selected size ranges of the synthetic normalized biomass size spectra (NBSS). PPMRs calculated as difference between $M_{0\_predator}$ and M_{0_prey} which are calculated according to Equation (6), individual statistics for dome-shaped patterns not presented.
Abbreviations: mesopFish, mesopelagic fishes; MicNek, micronekton; n.d.p, no dome present; uvpZPL, UVP-measured zooplankton; ZPL, zooplankton.

TABLE 7 Comparison of ensemble mean normalized biomass size spectra (NBSS) slopes for single ecosystem components or the phytoplankton–zooplankton aggregate from different studies, and methodological characteristics of each study.

Type and reference	Ecosystem components	Day (D)–Night (N) sampling	maxDepth (m)	NBSS slope mean/ range and biomass units	Comment
Single ecosystem components					
This study	PPL	...	2–200	C: −1.37	
González-García et al. (2023)	PPL	...	2–200	C: ~−0.8 to −1.1 (~−0.2 to −1.8)	Their Figure 7c (and total range)
This study	ZPL	N	200–1000	C: −0.92	
Couret et al. (2023)	ZPL	N	200	C: −074 to −0.84	3 regions incl. coastal upwelling
de Figueiredo et al. (2025)	ZPL	D/N mean	200	Vol: −0.82 to −0.95	Detailed study on the Brazilian shelf and oceanic islands
This study	Total micronekton	N	0–800	C: −1.28	
Two or three plankton ecosystem components					
This study	PPL–ZPL	N	200–1000	C: −0.91 Vol: −0.87	See Table 2 models 31 and 32
Quinones et al. (2003)	BPL–PPL–ZPL	N	400	C: −1.14 Vol: −0.99	Only oligotrophic regions
Martin et al. (2006)	PPL–ZPL	N	50	C: −1.07 to −1.10	
Stukel et al. (2024)	PPL–ZPL	D/N mean	100–200	C: −1.16 to −1.61	
Lombard et al. (2024)	PPL–ZPL	N	500	C: NA Vol: −0.8 to −0.9	Few samples only, their figs. S3 and S5

Abbreviations: BPL, bacterioplankton; C/Vol, biomass estimates based on carbon or biovolume; maxDepth, deepest depth of plankton sampling; PPL, phytoplankton; ZPL, zooplankton.

regions of the Sargasso Sea and subtropical seamounts and included bacterioplankton in their analysis. The extreme oligotrophic environment affected their slopes to become steeper, that is, phytoplankton as well as phytoplankton–zooplankton slopes steepen with decreasing primary production (González-García et al., 2023; Stukel et al., 2024). The inclusion of bacterioplankton resulted in a further offset of about five log2 units in relation to phytoplankton (Quinones et al., 2003), which would also steepen slopes. Focusing on the ocean surface layer (Martin et al., 2006) or including day samples (Stukel et al., 2024) leads to down-weighting of a considerable portion of migrating and larger zooplankton biomass, thus leading to steeper slopes of <-1. For the nCCUS region in this study, Couret et al. (2023) showed that daytime slopes were significantly steeper and daytime zooplankton assemblages had a less diverse composition as compared to night tows.

Between TLs: Three ecosystem components

Spatially, averaging was applied to obtain geographic patterns (Couret et al., 2023; Fock & Czudaj, 2019; Lira et al., 2024; Sheldon et al., 1972; Zhou & Huntley, 1997). Gaedke (1992) assigned differences between seasonally and annually averaged plankton spectra of Lake Constance to differences in intrinsic reactions of the ecosystem components to seasonal perturbations; thus, averaging was supposed to eliminate irregularities on a smaller scale caused by these perturbations. In the same way, the averaging of samples was supposed to eliminate the seasonal effect observed in the Benguela micronekton assemblage (Fock et al., 2025) or in marine plankton of Georges Bank, Northwest Atlantic (Boudreau & Dickie, 1992). Hatton et al. (2021) extended this concept aiming at obtaining a global size spectrum built on statistical models of the ecosystem components in relation to environmental drivers, except for mesopelagic fish that were modeled by FISHMIP. In the present study, Table 1 and Figure 2 show that components were neither sampled in the same place nor at the same time; hence, referring to the perturbation argument, the calculation of an ensemble mean slope to indicate the mean state of all seven regions combined appears justified. For phytoplankton, likely some of the seasonality is captured, for instance in the Benguela (SBUS month 2, NBUS month 10), or oceanic regions OMZ_sCCUS, EQU, and nCCUS, during months 1, 5, and 12. In contrast, no seasonal duplicates were taken for mesopelagic fishes and total micronekton except for the BUSs. Seasonality in the regions ranges from weak (EQU, nCCUS) to strong (NBUS, SBUS) (Longhurst, 2007; Pérez et al., 2005).

Considering three ecosystem components, the present study shows that calculating slopes from PPL–ZPL–micNek including conversions for the latter deemed reasonable to account for sampling biases resulted in values from −0.866 to −0.894 (Table 2, models 27 and 28), fairly close to PPL–ZPL slopes of −0.869 and −0.907 (Table 2, models 31 and 32). This would suffice the MTE proposition of a common slope across TLs. Furthermore, these slopes were significantly larger than the suggested "typical" slope of approximately −1.05 (Barnes et al., 2010; Hatton et al., 2021; Hunt et al., 2015; Trebilco et al., 2013), or observed marine slopes of −1.04 to −1.07 (Boudreau & Dickie, 1992) and for lakes, ranging from −1.02 to −1.11 (Yurista et al., 2014) or −1.13 to −1.21 (Mehner et al., 2018). A look at the original publication of Sheldon et al. (1972) may help resolve the discrepancies at least for the marine systems. Sketching their hypothesis for the EQU Pacific, Sheldon et al. (1972) developed a model with standing stocks of phyto- and zooplankton, micronekton, and tuna with a normalized slope of approximately −1.01. Plankton was collected either by bucket sampling from the surface or by water pumping from 4 m. Gelatinous zooplankton and nauplii are sensitive to pump sampling, leading to some sampling bias (Sameoto et al., 2000). Micronekton and tuna values were based on net sampling. Their micronekton value may be considered equivalent to "micronekton as is" in this study, and the tuna value was considered underestimated already in the original publication. Tentatively applying the conversions to micronekton as done in this study to overcome some of the sampling bias increases their slope to >-1 for three ecosystem components: phytoplankton, zooplankton, and micronekton. This effect of applying conversions is clearly depicted in Table 2, and the effect of various sampling methodologies on the difference of slopes between UVP-sampled and net-sampled zooplankton. Hence, the differences to Boudreau and Dickie (1992) and to Sheldon et al. (1972) can likely be attributed to improved sampling methodologies for zooplankton and micronekton.

Ensemble mean slopes by biovolume were larger than those calculated for carbon contents (Quinones et al., 2003). Lombard et al. (2024) showed that considering bacterio-, phyto-, and zooplankton, the percentage of shallow slopes by biovolume strongly increased as compared to carbon biomass slopes. In this study, best models in terms of AIC (Table 2, models 27 and 28) indicated that the biovolume ensemble mean slope was not significantly larger than the carbon biomass slope (Table 2, z), but both were larger than the MTE-predicted theoretical slope of −1. The biovolume slope of −0.866 indicates that biomass B (rather than $B(M)$) scales with $M^{0.134}$, that is, biomass increases with body mass and the biomass pyramid is inverted (Trebilco et al., 2013).

The microbial loop and pelagic community structure

The analysis of contrasts in relation to primary production revealed that the microbial loop is supposed to deliver important contributions to the pelagic food web, particularly at low levels of primary production. Generally, two pathways of autotrophic carbon entering the heterotrophic food web can be considered, that is, either through direct grazing on phytoplankton or through exudation of DOM and subsequent consumption by bacteria (Gaedke, 1993). For lake systems, bacteria contributed less to carbon turnover than would be expected from their spectral densities, given that bacterial metabolic rate did not follow metazoan allometric metabolic rules under food limitation (Gaedke, 1993). The resulting spectrum was without positive offset for zooplankton, as shown in this study. Likewise, in food web studies of three of the Great Lakes, no zooplankton offset in terms of an "inverted" size distribution was indicated, analyzing NBSS for the components phytoplankton–zooplankton–fish (Sprules & Goyke, 1994; Yurista et al., 2014). For two other German lakes, Mehner et al. (2018) analyzed NBSS from bacteria to macrozoobenthos (fishes not included in their *lme* model) and found a negative offset for zooplankton (−1.81 as residuals on a log2-scale as compared to 0.05 for phytoplankton and 0.24 for macrozoobenthos, though not exactly the same as a population marginal mean). In line with this observation, for three Canadian lakes not included in the Great Lakes studies, negative zooplankton offsets were indicated (Giacomini et al., 2023, fig. E1). Contrary to these findings, our synthetic NBSS indicated a significant positive offset for zooplankton, both for ZPL and for uvpZPL (Figure 5a–d), pointing to a fundamental difference between lake and ocean systems. Particle densities in terms of uvpZPLD were even higher, as indicated in the analysis of biovolume NBSS marginal means (Figure 5c). Contrasts for PPL–uvpZPL and PPL–uvpZPLD were correlated to primary production in the same way, indicating that the zooplankton ecosystem component was linked to the concentration of zooplankton and detritus (Figure 6b, Tables 4 and 5). With one data point missing (OMZ_sCCUS), the PPL–ZPL contrasts showed a similar pattern and were always negative, although for EQU close to parity (Figure 8 a, contrast = −0.09). It is noteworthy that the EQU ZPL and nCCUS ZPL were sampled with 200-µm WP-2 nets and that more samples were available for uvpZPL than for ZPL.

The major difference between freshwater and marine NBSS regarding the zooplankton offset is not likely attributed to the presence of particulate organic matter (POM) as such, since lake POM occurs in similar concentrations as marine POM (Grossart & Simon, 1993, 1998) and bacterial abundance can even be higher in freshwater systems than in marine systems (Simon et al., 1992). In both lake and ocean systems, pelagic bacterial production (BP) is linearly related to net primary production (NPP) with BP-NPP slopes ~1 in both systems (Cole et al., 1988). However, both systems differ in terms of carbon origin and utilization. $\delta^{13}C$ analysis of micro- and macrozooplankton revealed differences in ^{13}C enrichment between freshwater and marine systems with a significant correlation to POM $\delta^{13}C$ (Del Giorgio & France, 1996). Marine POM and zooplankton $\delta^{13}C$ ranged from −17‰ to −25‰ in line with recent measurements (Hansman & Sessions, 2016), while for lake zooplankton, values ranged from −25‰ to – 40‰. One possible explanation was that ^{13}C-enriched surface water layers indicative of algal carbon input to the zooplankton assemblage were only very shallow in the order of meters in lake systems (epilimnion) as compared to 10^2–10^3 m in marine systems so that the access for vertically migrating zooplankton to algal carbon and algal-derived POM of the microbial food web in both systems is quite different (Del Giorgio & France, 1996). For limnetic systems, the separation of epi- and hypolimnetic carbon pathways is supported by Zimmer et al. (2020), and up to 80% of carbon respired by epilimnetic bacteria has a non-algal origin (McCallister et al., 2008). In slight support of this rationale in the marine realm, Gloeckler et al. (2018) showed that at the station ALOHA off Hawaii, the $\delta^{15}N$ signature of surface waters extended to >200-m depth. Accordingly, Del Giorgio and France (1996) showed that for eutrophic lakes with a higher share of algal carbon, the zooplankton $\delta^{13}C$ signature became similar to that of marine zooplankton, underpinning that lake zooplankton preferred algal ^{13}C over non-algal ^{13}C. In open-ocean systems without terrigenous carbon input, degradation of POM can follow manifold pathways depending on the colonization of POM with various microbial components and associated subsequent feeding and respiration (Iversen, 2023). While respiration delivers $\delta^{13}C$-depleted carbon dioxide, POM is enriched in $\delta^{13}C$. For example, $\delta^{13}C$ of marine POM increased from −23‰ in the surface layer to −20‰ in the depth range 800–1000 m at a Pacific site (Yang et al., 2017).

Hence, we conclude that the better access to algal carbon could explain that open-ocean systems support more heterotrophic biomass than lake systems do for a given algal biomass and that the imbalance in favor of zooplankton biomass ("top-heaviness") increases with decreasing autotrophic biomass and thus increased POM production in the open ocean (Gasol et al., 1997). The vertical dimension for marine mesopelagic systems is 10^3 m as compared to 10^1–10^2 m for lake systems, thus

providing more space and time for interactions, and the flux into the benthic system that could be responsible for negative offsets of lake zooplankton declines with depth in the ocean water column (Engel et al., 2017). In turn, dependence on particle and/or nitrogen flux was shown for the epi- and mesopelagic vertical distribution of an abundant group of marine unicellular zooplankton, that is, Rhizaria (Barth et al., 2024). DOM production and export as a precursor to POM globally is the highest in oligotrophic regions (Roshan & DeVries, 2017). This is mirrored through correlations between primary production and contrasts for PPL–ZPL (Figure 8a), PPL–uvpZPL, and PPL–uvpZPLD, of which correlations related either to uvpZPL or to uvpZPLD were significant (Figure 6b, Table 5). POM in turn is a highly dynamic substrate. Its availability is strongly modified through phytoplankton community structure and vertical hydrography. Large phytoplankton cells enhance POM export (Boyd & Trull, 2007) as does reduced midwater oxygen content. Particle flux is in particular high in OMZ regions where low oxygen concentrations hamper microbial turnover in the midwater OMZ, thus providing significant carbon input to deeper waters (Devol & Hartnett, 2001; Engel et al., 2017; Moigne et al., 2017; Soviadan et al., 2022). POM stability is modified through microbial composition and zooplankton interactions. Aggregates can attract microorganisms, reducing the stickiness with hydrolases or increasing it by mucus production (Azam & Malfatti, 2007). Zooplankton may interact with POM and modify POM flux through grazing, aggregation of smaller particles into larger fecal pellets, fragmentation of larger particles, active vertical transport, and flux feeding while intercepting the sinking particles with external filtering nets (Iversen, 2023). The averaging approach over depth and space applied in this study likely levels out these contrasting processes so that the correlation results appear consistent to indicate top-heaviness, that is, in particular negative contrasts to PPL in Figure 6 for uvpZPL, mesopelagic fishes, and micronekton. In turn, the aspect of feeding interactions highlights that those differences in zooplankton community composition between lake and ocean systems could be important as well. The ecological niche of microphagous gelatinous-like plankton in lake systems is mainly occupied by microzooplankton, that is, rotifers (Dumont, 2007; Lüskow et al., 2024), while marine microphages also belong to macro- and megaplankton and are accounted for here as part of the zooplankton and micronekton because of their size. Thus, with delimited interactions for lake macrozooplankton towards POM, a preference for algal carbon prevails and Mehner et al. (2022) concluded that only little carbon enters the lake food web via the microbial loop.

For mesopelagic fishes, compound-specific $\delta^{15}N$ analysis allows for the determination of the contribution of the microbial community to feeding, which is estimated at about 20% both for DVM migrators and for non-migrators (Bode et al., 2021). Gloeckler et al. (2018) further indicated that the attribution from the microbial food web is dynamic, that is, a shift in the selection of carbon from larger to smaller sized POM is correlated with depth. In line with the former, estimated mean marginal spectral densities for mesopelagic fishes are not different from phytoplankton marginal means, which is thus supposed to contribute the bulk of carbon input into this ecosystem component (Figure 4a–c). In line with the latter, the correlation of the PPL–mesopFish contrasts with primary production (Figure 6a,c) shows that the selection of food source may be dynamic. Under oligotrophic conditions, the spectral densities of mesopelagic fishes are higher than would be expected from phytoplankton alone, likely indicating input from the microbial loop, while under eutrophic conditions, this relationship is reversed. Davison et al. (2015) modeled that mesopelagic fishes consumed about 90% of the NPP in oligotrophic waters, which was considered unrealistic, decreasing to <20% when primary production reaches 1000 mg C m^{-2} day^{-1}. They discussed further input from the microbial loop to be required in oligotrophic environments. As such, Pomeroy et al. (2007) stated that in oligotrophic marine systems the versatility of the microbial loop is essential to sustain fish production. Under eutrophic conditions, typically altricial and short-lived mesopelagic fishes with a low fecundity (Knorrn et al., 2024; Merrett, 1994) are probably outcompeted by fast-growing gelatinous micronekton and by migrating shelf fishes with high fecundity. In turn, this shift in ecosystem structure is further evident from contrasts mesopFish–ZPL (Figure 8b) and mesopFish–uvpZPL (Figure 8d), which are relatively small under oligotrophic conditions but increase with primary production in favor of zooplankton, that is, contrasts mesopFish–ZPL were on average −0.35 for the oligotrophic habitats BRZ_oc_isl, BRZ_shlf, and EQU. This indicates that mesopelagic fishes constituted about half of the normalized biomass that would be expected from zooplankton spectral densities after applying micronekton conversions for trawl type and volumetric–gravimetric differences in biovolume calculations. Because of the missing conversion for hydroacoustic biomass, Figure 8b is considered less likely (see Figure 8c) as compared to the relationship in Figure 8d.

Both figures for mesopelagic fishes and total micronekton in relation to uvpZPL for all seven regions (Figure 8d,e) and for ZPL where negative contrasts are obtained in relation to ZPL (Figure 8c) indicate a surplus of zooplankton over micronekton and thus a break in the

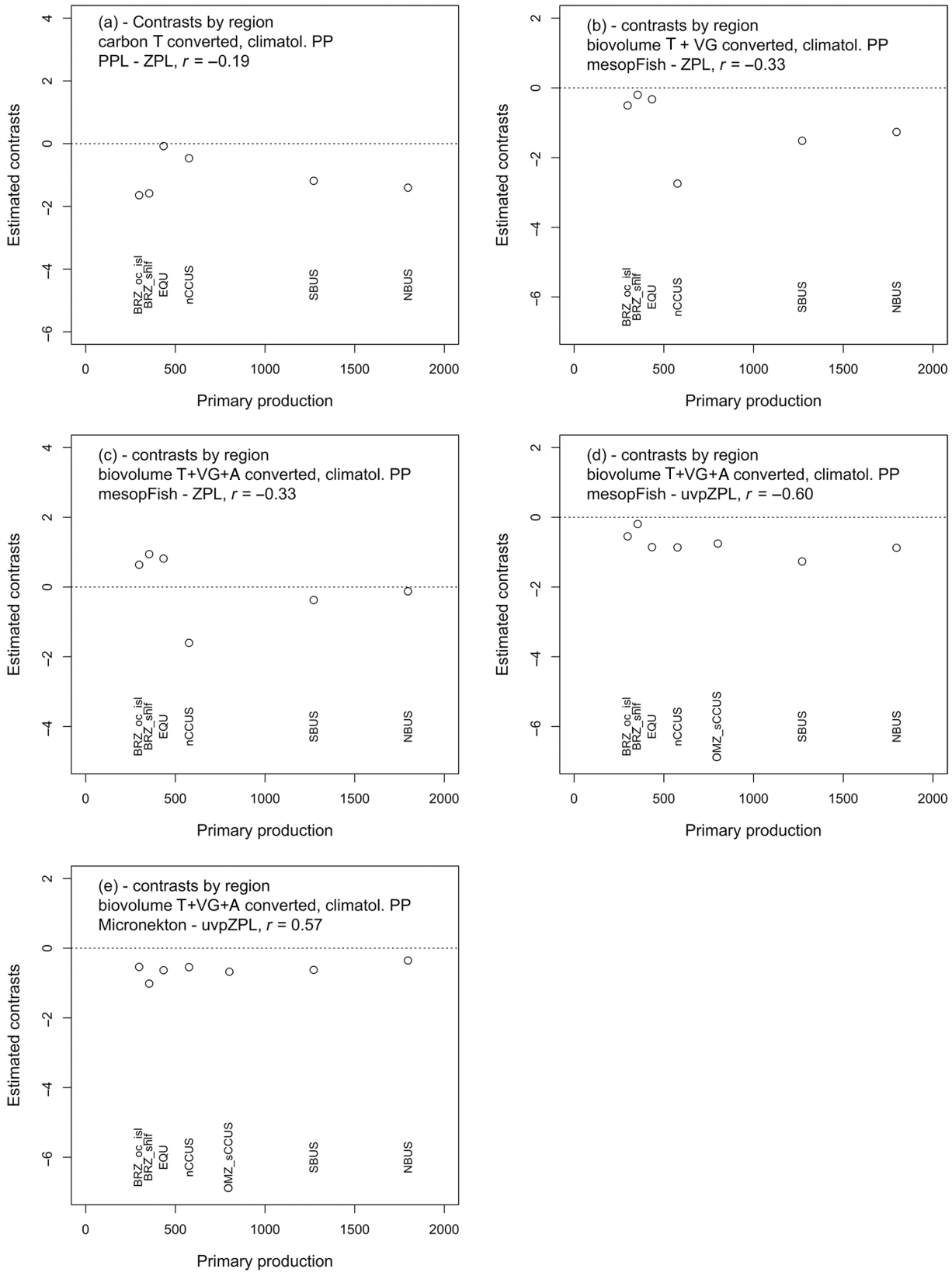

FIGURE 8 Biomass ratios between ecosystems components on $\log_{10}$-scale, that is contrasts, (a) phytoplankton and net zooplankton for carbon biomass, (b, c) mesopelagic fishes and net zooplankton for biovolume in relation to primary production with two different conversions, (d) mesopelagic fishes and UVP-measured zooplankton (uvpZPL) for biovolume, and (e) micronekton and uvpZPL for biovolume. Negative values indicate higher zooplankton spectral density as compared to phytoplankton or mesopelagic fishes. No ZPL data for southern Canary Current Upwelling System oxygen minimum zone (OMZ_sCCUS). Micronekton conversions indicated. Climatol. PP, primary production as climatological mean in milligrams of carbon per meter squared per day. For region abbreviations, see Figure 6.

structure of the synthetic NBSS. In a reversal of the interpretation of inverted biomass pyramids, namely that always two types of food sources feed into a top-heavy ecosystem component (Trebilco et al., 2013), the steep decline from zooplankton to mesopelagic fishes could indicate that zooplankton may have two groups of predators, of which only one is captured in this analysis. Further missing components in the NBSS analysis are both demersal fish and genuine epipelagic constituents. The argument of missing demersal fishes would apply to the Brazilian shelf habitat. For oceanic regions, biomass estimates of epipelagic fishes range from about 10% of the mesopelagic fish biomass (Lehodey et al., 2010; Maury, 2010) equivalent to a contrast of about −0.05 to about 200% (Calhoun-Grosch et al., 2024) equivalent to a contrast of 0.35, the latter percentage as a ratio of complete living biomasses in both subsystems. In turn, our contrasts of <−1 for the highly productive regions, indicating a >10-fold difference (Figure 8b,d,e, similarly for total micronekton and uvpZPL), cannot be directly explained by missing ecosystem components. This underpins that the understanding of mesopelagic carbon dynamics remains incomplete with expected local and regional differences in sources (Bode et al., 2021; Gloeckler et al., 2018). Accordingly, responses in terms of differential contrasts in relation to primary production are shown here. This could be essential to improving predictions of future pelagic biomass yields from size spectra properties, for example, Atkinson et al. (2024).

Interpretation of the functional advantage of biovolume over carbon biomass and implications for TTE

In this study, the choice of biomass unit—either biovolume or carbon content—affected PPMRs and had a significant effect on NBSS slopes, the latter indicating that biovolume spectra were more top-heavy than spectra based on carbon content. This to some degree is related to gelatinous zooplankton (Lombard et al., 2024) and gelatinous micronekton, for which carbon conversion factors needed to be applied to account for the higher water contents of their tissues (see *Materials and methods*). Gelatinous plankton is a heterogeneous group spanning from herbivores (*Pyrosoma* spp.) to top predators (Ctenophora) and is characterized by accordingly varying PPMRs and high growth rates corresponding to large body sizes and short lifespans (Chi et al., 2021; Jaspers et al., 2023; Pitt et al., 2013). Recently, Rhizaria, also gelatinous when considering their mucus, have been shown to flatten the NBSS in surface and mesopelagic layers mostly of the inter-tropical ocean, contributing also to the differences between NBSS expressed in volume and carbon (Soviadan et al., 2024).

MTE makes the proposition of a common NBSS slope across all ecosystem components considered. The similarity of slopes of two components, PPL–ZPL on one side and of three components PPL–ZPL–micNek with fully converted micronekton on the other side, is in support of this proposition (Table 2). Thus, the MTE term for the NBSS slope: $\gamma + 0.75 = \log_{10}(\mathrm{TTE})/\log_{10}(\mathrm{PPMR})$, can be applied to interpret differences between spectra in terms of trophic efficiency TTE for either biomass unit applied, keeping in mind that the biovolume slope is the "true" slope, while the carbon slope is converted from biovolume or from weight. TTE may not exceed the gross growth efficiency (GGE) of the populations involved (Davison et al., 2013). GGE is defined as the amount of consumer carbon produced relative to the amount of prey ingested in a given time interval. The range of observed GGE for zooplankton is 20%–30% (Straile, 1997) and for mesopelagic fishes 24%–52% (Childress et al., 1980). Gelatinous zooplankton with a much higher carbon-specific growth rate as compared to fish may have even higher values, bearing the advantage of "low construction costs" (Pitt et al., 2013).

The MTE approach is sensitive to the calculation of PPMR (Eddy et al., 2021), which we did according to the BDKT model. The zooplankton–mesopelagic fishes' PPMR as taken from Table 4 ranged from a median of 5900:1 for oceanic habitats to 437:1 for coastal and island habitats. Furthermore, PPMRs may also change between adjacent TLs (Barnes et al., 2010). Applying the MTE approach, Barnes et al. (2010) calculated a TTE of 13.4% for a PPMR of 800:1 and a "typical" slope of −1.05. Similar to our study, Hunt et al. (2015) calculated micronekton/mesopelagic fishes' PPMRs ranging from 204:1 to 3863:1, while for mesozooplankton, the range was 389:1 to 10,099:1, resulting in lower TTE between phyto- and zooplankton, altogether with TTEs < 10%. Otto et al. (2007) showed that in five empirical food webs, pairwise PPMRs ranged between 10^8:1 and <1. With a constant TTE, both very high and PPMR < 1 could lead to an increase in the NBSS slope to values >−1. Table 4 shows that carbon-based PPMR were larger than PPMR based on biovolume. Hence, biovolume PPMR could influence the PPMR distribution in both directions, that is, towards very high values if the link to smaller crustacean prey is considered, and to values <1 if low-carbon volume-rich gelatinous predators become capable of feeding on smaller carbon-rich mesopelagic fishes or larvae.

PPMR was calculated between the ecosystem components ZPL and mesopelagic fishes. Carbon-based TTEs ranged from 28.9% for open-ocean habitats to 41.9% for

coastal/island habitats for the two ecosystem components considered, while the respective biovolume TTEs ranged from 36.8% to 49.7%. Given that the slopes of models 27 and 28 (Table 2) were not significantly different, the TTE values can be understood as ranges for the open ocean (28.9%–36.8%) and coastal/island habitats (41.9%–49.7%). Based on the shallower slopes for the BRZ_oc_isl system as compared to the BRZ_shlf habitat (Appendix S6: Tables S1 and S2), de Figueiredo et al. (2025) suggested a further differentiation within the coastal/island habitats with increasing TTE from shelf to oceanic islands.

The biovolume system tends to have a higher TTE and that TTE is notably higher than 10%, that is, close to the maximum set by known GGEs. Davison et al. (2013) discussed that a TTE of 10% was not sufficient to sustain mesopelagic biomass in the oceans and suggested TTEs of 30%, including transfer through the microbial loop. With regard to the biovolume argument, increased trophic efficiency was evidenced for the gelatinous zooplankton (Havens et al., 2000; Jaspers et al., 2023; Kwong et al., 2022). These are capable of retaining small POC in mucus nets, and larvaceans may release up to 1000 mg C m^{-2} day^{-1} in terms of fecal pellets during phytoplankton blooms in the Benguela system (Ekau et al., 2018). Increased trophic efficiency and high growth rate of gelatinous plankton allow a reinterpretation of Figure 7b,d: The functional advantage of biovolume-based systems enables resource constraints imposed by limited productivity to be overcome by increasing local transfer efficiency so that the regional marginal means are no more related to primary production. Accordingly, the relationship between NBSS slope and productivity was not significant when considering biovolume (Figure 7c compared to Figure 7d). The same was shown for phytoplankton rendering phytoplankton biovolume independent of nutrient resources (Moreno-Ostos et al., 2015). The MTE provides a simple interpretation of this volume-based increase in transfer efficiency, based on the definition of TTE, that is, $TTE = N_1/N_0 \times (W_0/W_1)^{-0.75}$ (Brown et al., 2004, 1785), where subscripts 0 and 1 denote prey and predator, respectively. Considering that the ratio of abundances of predator and prey, N_1/N_0, is constant for a specific predator–prey constellation regardless of whether carbon biomass or biovolume is considered, the carbon-based transfer efficiency becomes $TTE_c = \text{const} \times \left({}^{c}W_0/{}^{c}W_1\right)^{-0.75}$. In terms of biovolume, doubling of predator size ${}^{\text{vol}}W_1$ relative to

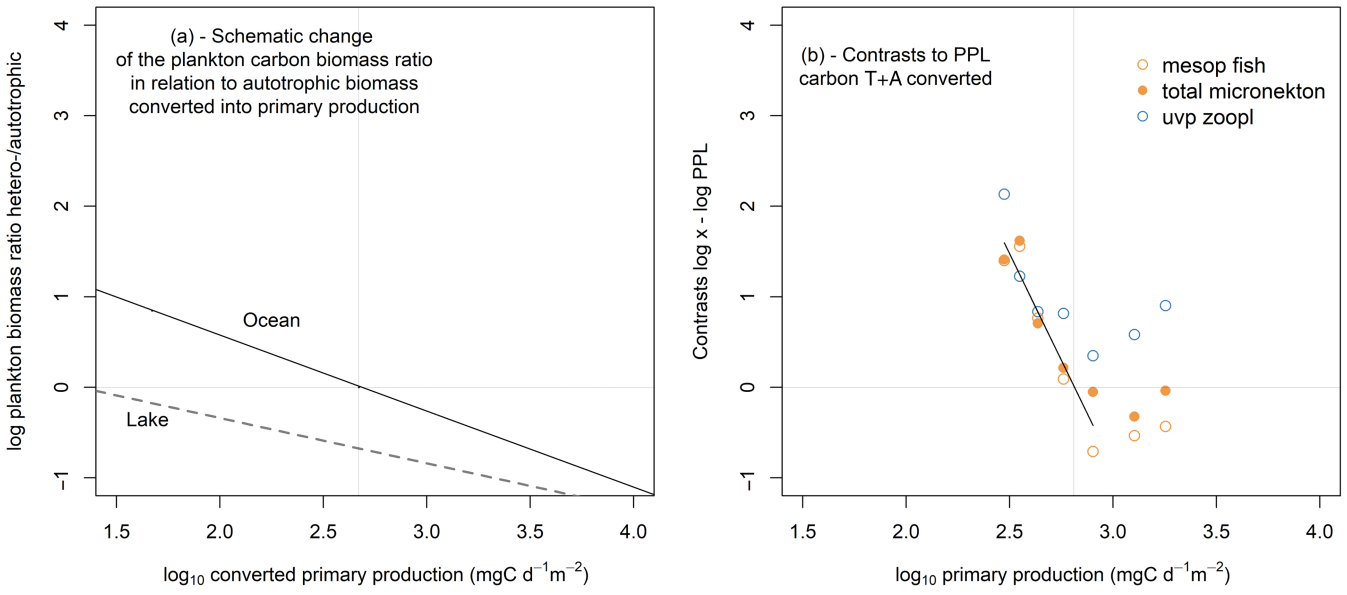

FIGURE 9 Comparison of (a) the extrapolated schematic plankton model of heterotrophic dominance in relation to phytoplankton biomass in aquatic ecosystems redrawn from Gasol et al. (1997: Figure 6 and Table 3) and (b) observed contrasts in relation to phytoplankton spectral densities across the primary production gradient (based on model 28, Table 2). Both figures are based on carbon biomass. Gasol et al. (1997) scaled the *x*-axis as phytoplankton biomass, but phytoplankton biomass is not the best parameter to estimate production/biomass ratios (*P*/*B*) and primary production. However, for the purpose of aligning (a) and (b) we take a phytoplankton *P*/*B* proxy for oligotrophic waters of 0.21 day^{-1} from Marañón et al. (2021) to convert the original phyoplankton biomass into primary production in (a). The intersection of the ocean regression line in (a) with the line $H/A = 1$, and of the micronekton and mesopelagic fishes' contrasts in (b) appear similar, that is, at 2.67 and 2.81, respectively, equivalent to 470 and 651 mg C m^{-2} day^{-1} (also see Figure 6c). Primary production as climatological mean in milligrams of carbon per meter squared per day. A, acoustic–trawl conversion; PPL, phytoplankton; T, trawl type conversion; uvp zoopl, UVP-measured zooplankton.

$^{vol}W_0$ and normalizing by TTE_c would improve the TTE_{vol} by a factor of 1.7; a fourfold increase in biovolume over carbon content would lead to an improvement by a factor of 2.8. This is likely not apparent, since many other parameters such as prey encounter rate for the gelatinous predator would also be influenced by size. This is exemplified by the definition of TTE of Sheldon et al. (1977) as the product of growth efficiency of the predator, GGE_{pred}, and the portion of the prey production it can consume, C_{prey}. With an increased encounter rate, more prey can be captured. If all prey production can be consumed ($C_{prey} = 1$), TTE equals GGE.

Food web modeling shows that with community biomass in terms of biovolume scaling at $M^{>0}$, as shown in this study, TTE > 0.2 can be achieved in such inverted communities at PPMRs of 2000 and higher (Trebilco et al., 2013) (their Arabian Sea food web example), while the overall global mean TTE in their compilation was 0.101 referring to the Pauly and Christensen (1995) ensemble of ecosystem studies. This interpretation of the relative increase of efficiency in biovolume systems as compared to carbon biomass—or allometric advantage sensu Pitt et al. (2013)—provides an alternative approach to explaining the preponderance of gelatinous zooplankton in ocean systems, while the classical jellification, that is mass developments of gelatinous organisms often in coastal regions for instance in the Benguela system, was attributed to overfishing (Roux et al., 2013), supposing that fish and jellyfish were strong competitors (Flynn et al., 2012).

CONCLUSIONS

Synthetic pelagic size spectra were applied to analyze changes in community structure and functioning in seven regions of the tropical and subtropical Atlantic. The first hypothesis (different slopes for biovolume- and carbon-based NBSS) could be supported only when using unconverted micronekton data and by ANOVA with interactions among biomass unit, region, and ecosystem component as factors. The second hypothesis (higher spectral densities for zooplankton relative to phytoplankton and log ratios of mean spectral densities, that is, contrasts, related to primary production) was also supported. Marginal mean spectral densities of both total micronekton and uvpZPL were significantly higher than for phytoplankton (Figure 5d), underpinning the importance of the energy flow through the microbial loop. Hence, the inclusion of microzooplankton and bacterial data, which were not available in this study, appears indispensable in the future to achieve a full living NBSS. A comparison with other studies of phytoplankton–zooplankton size spectra revealed similar results in support of the postulated role of the microbial loop (Table 5). Furthermore, both zooplankton (better for uvpZPL than for ZPL) and mesopelagic fishes and total micronekton showed a similar dominance pattern relative to phytoplankton at lower levels of primary production (Figures 6, 8, and 9b). This dominance of the heterotrophic pathway is evident in both the work of Gasol et al. (1997), where the heterotrophic pathway dominates below an estimated primary production threshold of approximately 470 mg C m^{-2} day^{-1} (Figure 9a), and in this study with a threshold of approximately 650 mg C m^{-2} day^{-1} (Figure 9b), the latter shown for uvpZPL, mesopelagic fishes, and micronekton contrasts in relation to phytoplankton. While in Figure 9a the regression lines of Gasol et al. (1997) were extrapolated beyond the original value range, this appears not well supported by the curves for uvpZPL, total micronekton, and mesopelagic fishes that all appear to reverse trends at primary production values larger than 650 mg C m^{-2} day^{-1} (Figure 9b). The third hypothesis (regional differences of size spectrum properties related to primary production) delivered significant results for slopes only if NBUS was removed. In turn, a significant correlation of regional marginal means with primary production was only revealed in the analysis of carbon biomass spectra, whereas for biovolume spectra, no relationship was found. This can be interpreted as a functional advantage of the biovolume system to increase TTE independent of its carbon biomass. Ensemble mean NBSS slopes were significantly larger than −1, indicating that with improved modern sampling techniques, Sheldon and Parsons (1967) and Sheldon, Prakash, and Sutcliffe's (1972) statement of "roughly equal concentration of material ... at all particle sizes" requires revision. Looking at climate change, with projected ocean phytoplankton biomass declining under all climate change scenarios (Lotze et al., 2019), this allows one to predict future oceanic pelagic community organization, that is, a shift towards higher contrasts in relation to phytoplankton (Figure 9b).

AUTHOR CONTRIBUTIONS

Conceptualization, formal analysis, visualization, writing—original draft: Heino O. Fock, Arnaud Bertrand, Emilio Marañón, Lars Stemmann, Ralf Schwamborn. *Investigation and data curation*: Heino O. Fock, Henrike Andresen, Arnaud Bertrand, Gabriel Bittencourt Farias, Claire Carré, María Couret, Javier Díaz-Pérez, Tim Dudeck, Mathilde Dugenne, Sabrina Duncan, Gabriela Guerra Araújo Abrantes Figueiredo, Thierry Frédou, Flávia Lucena-Frédou, Xiomara F. G. Díaz, Dawit

Yemane, Cristina González-García, Rainer Kiko, José M. Landeira, Simone M. A. Lira, Florian Lüskow, Emilio Marañón, Pedro Augusto Mendes de Castro Melo, Sigrid Neumann-Leitao, Leandro Nole Eduardo, Lars Stemmann, Ralf Schwamborn. *Writing—review and editing*: Heino O. Fock, Henrike Andresen, Arnaud Bertrand, Gabriel Bittencourt Farias, Claire Carré, María Couret, Javier Díaz-Pérez, Tim Dudeck, Mathilde Dugenne, Sabrina Duncan, Gabriela Guerra Araújo Abrantes Figueiredo, Thierry Frédou, Flávia Lucena-Frédou, Xiomara F. G. Díaz, Dawit Yemane, Cristina González-García, Rainer Kiko, José M. Landeira, Simone M. A. Lira, Florian Lüskow, Emilio Marañón, Pedro Augusto Mendes de Castro Melo, Sigrid Neumann-Leitao, Leandro Nole Eduardo, Lars Stemmann, Ralf Schwamborn.

ACKNOWLEDGMENTS

We are grateful to the Federal Ministry of Education and Research (BMBF) for funding the TRAFFIC project under the SPACES II research program for SD (project funding number: 03F0797D) and TD (03F0797A). Henrike Andresen, Simone M. A. Lira, Ralf Schwamborn, Rainer Kiko, Javier Díaz-Pérez, Tim Dudeck, and Cristina González-García were supported through the TRIATLAS project of the European Union's Horizon 2020 research and innovation program under grant agreement number 817578EU H2020. José M. Landeira was funded by the DESAFIO project (reference: PID 2020-118118RB-100) of the Spanish Ministry of Science and Technology, and IMDEEP (CajaCanarias-LaCaixa, reference: 2022CLI SA15). Rainer Kiko and Mathilde Dugenne acknowledge funding from NOAA (award number NA21OAR4310254) for the "Developing PSSdb: a Pelagic Size Structure database to support biogeochemical modelling" project. Rainer Kiko furthermore acknowledges funding from the Heisenberg Program of the German Science Foundation number KI 1387/5-1. María Couret was supported by a postgraduate grant (TESIS2022010116) co-financed by the Agencia Canaria de Investigación, Innovación y Sociedad de la Información de la Consejería de Universidades, Ciencia e Innovación y Cultura and by the Fondo Social Europeo Plus (FSE+) Programa Operativo Integrado de Canarias 2021-2027, Eje 3 Tema Prioritario 74 (85%). Javier Díaz-Pérez was supported by the "ULPGC2022-2" grant from Universidad de Las Palmas de Gran Canaria. The ABRAÇOS surveys were funded by the French Oceanographic fleet; this work is a contribution to the IJL TAPIOCA. Open Access funding enabled and organized by Projekt DEAL.

CONFLICT OF INTEREST STATEMENT

The authors declare no conflicts of interest.

DATA AVAILABILITY STATEMENT

Data (Fock et al., 2024) are available from Zenodo: https://doi.org/10.5281/zenodo.13627093.

ORCID

Heino O. Fock https://orcid.org/0000-0003-2902-3559
Henrike Andresen https://orcid.org/0000-0001-8836-6370
Arnaud Bertrand https://orcid.org/0000-0003-4723-179X
Gabriel Bittencourt Farias https://orcid.org/0000-0002-5287-5082
Javier Díaz-Pérez https://orcid.org/0000-0002-7268-4398
Xiomara F. G. Díaz https://orcid.org/0000-0002-6140-5373
Rainer Kiko https://orcid.org/0000-0002-7851-9107
José M. Landeira https://orcid.org/0000-0001-6419-2046
Florian Lüskow https://orcid.org/0000-0002-2100-7012
Emilio Marañón https://orcid.org/0000-0003-1572-2121
Pedro Augusto Mendes de Castro Melo https://orcid.org/0000-0002-4117-239X
Leandro Nole Eduardo https://orcid.org/0000-0003-2369-4175
Lars Stemmann https://orcid.org/0000-0001-8935-4531
Ralf Schwamborn https://orcid.org/0000-0001-9150-8720

REFERENCES

Allen, A. P., J. H. Brown, and J. F. Gillooly. 2002. "Global Diversity, Biochemical Kinetics, and the Energetic-Equivalence Rule." *Science* 297: 1545–48.

Álvarez, E., Á. López-Urrutia, and E. Nogueira. 2008. "Nano- and Microplankton Size-Structure during Late Summer in the Southern Bay of Biscay." *Revista de Investigación Marina* 3: 217–18.

Andersen, K. H., T. Berge, R. J. Gonçalves, M. Hartvig, J. Heuschele, S. Hylander, N. S. Jacobsen, et al. 2016. "Characteristic Sizes of Life in the Oceans, from Bacteria to Whales." *Annual Review of Marine Science* 8: 217–241.

Andersen, K. H., J. E. Beyer, and P. Lundberg. 2009. "Trophic and Individual Efficiencies of Size-Structured Communities." *Proceedings of the Royal Society B: Biological Sciences* 276(1654): 109–114. https://doi.org/10.1098/rspb.2008.0951.

Arim, M., M. Berazategui, J. M. Barreneche, L. Ziegler, M. Zarucki, and S. R. Abades. 2011. "Determinants of Density-Body Size Scaling Within Food Webs and Tools for Their Detection." *Advances in Ecological Research* 45: 1–39. https://doi.org/10.1016/B978-0-12-386475-8.00001-0.

Atkinson, A., A. G. Rossberg, U. Gaedke, G. Sprules, R. F. Heneghan, S. Batziakas, M. Grigoratou, E. Fileman, K. Schmidt, and C. Frangoulis. 2024. "Steeper Size Spectra with Decreasing Phytoplankton Biomass Indicate Strong Trophic Amplification and Future Fish Declines." *Nature*

Communications 15(1): 381. https://doi.org/10.1038/s41467-023-44406-5.

Azam, F., and F. Malfatti. 2007. "Microbial Structuring of Marine Ecosystems." *Nature Reviews Microbiology* 5(10): 782–791. https://doi.org/10.1038/nrmicro1747.

Barnes, C., D. Maxwell, D. C. Reuman, and S. Jennings. 2010. "Global Patterns in Predator-Prey Size Relationships Reveal Size Dependency of Trophic Transfer Efficiency." *Ecology* 91(1): 222–232. https://doi.org/10.1890/08-2061.1.

Bar-On, Y. M., and R. Milo. 2019. "The Biomass Composition of the Oceans: A Blueprint of Our Blue Planet." *Cell* 179(7): 1451–54. https://doi.org/10.1016/j.cell.2019.11.018.

Barth, A., L. Blanco-Bercial, R. Johnson, and J. Stone. 2024. "Rhizaria in the Oligotrophic Ocean Exhibit Clear Temporal and Vertical Variability." *Deep-Sea Research Part I: Oceanographic Research Papers* 212(July): 104371. https://doi.org/10.1016/j.dsr.2024.104371.

Bates, D., M. Mächler, B. Bolker, and S. Walker. 2015. "Fitting Linear Mixed-Effects Models Using lme4." *Journal of Statistical Software* 67 (1 SE-Articles) (urriak 7): 1–48. https://doi.org/10.18637/jss.v067.i01.

Bertrand, A. 2015. "ABRACOS Cruise, RV Antea." https://doi.org/10.17600/15005600

Bertrand, A. 2017. "ABRACOS 2 Cruise, RV Antea." IRD. https://doi.org/10.17600/17004100

Bisson, K. M., R. Kiko, D. A. Siegel, L. Guidi, M. Picheral, E. Boss, and B. B. Cael. 2022. "Sampling Uncertainties of Particle Size Distributions and Derived Fluxes." *Limnology and Oceanography: Methods* 20(12): 754–767. https://doi.org/10.1002/lom3.10524.

Blanco, J. M., F. Echevarría, and C. M. García. 1994. "Dealing with Size-Spectra: Some Conceptual and Mathematical Problems." *Scientia Marina* 58(1–2): 17–29.

Bode, A., M. P. Olivar, and S. Hernández-León. 2021. "Trophic Indices for Micronektonic Fishes Reveal their Dependence on the Microbial System in the North Atlantic." *Scientific Reports* 11(1): 8488. https://doi.org/10.1038/s41598-021-87767-x.

Boudreau, P. R., and L. M. Dickie. 1992. "Biomass Spectra of Aquatic Ecosystems in Relation to Fisheries Yield." *Canadian Journal of Fisheries and Aquatic Sciences* 49(8): 1528–38. https://doi.org/10.1139/f92-169.

Boudreau, P. R., L. M. Dickie, and S. R. Kerr. 1991. "Body-Size Spectra of Production and Biomass as System-Level Indicators of Ecological Dynamics." *Journal of Theoretical Biology* 152(3): 329–339. https://doi.org/10.1016/S0022-5193(05)80198-5.

Boyd, P. W., and T. W. Trull. 2007. "Understanding the Export of Biogenic Particles in Oceanic Waters: Is There Consensus?" *Progress in Oceanography* 72(4): 276–312. https://doi.org/10.1016/j.pocean.2006.10.007.

Brown, J. H., and J. F. Gillooly. 2003. "Ecological Food Webs: High-Quality Data Facilitate Theoretical Unification." *Proceedings of the National Academy of Sciences* 100(4): 1467–68. https://doi.org/10.1073/pnas.0630310100.

Brown, J. H., J. F. Gillooly, A. P. Allen, V. M. Savage, and G. B. West. 2004. "Toward a Metabolic Theory of Ecology." *Ecology* 85(7): 1771–89. https://doi.org/10.1890/03-9000.

Burnham, K. P., D. R. Anderson, and K. P. Huyvaert. 2011. "AIC Model Selection and Multimodel Inference in Behavioral Ecology: Some Background, Observations, and Comparisons." *Behavioral Ecology and Sociobiology* 65(1): 23–35. https://doi.org/10.1007/s00265-010-1029-6.

Calhoun-Grosch, S., J. J. Ruzicka, K. L. Robinson, V. H. Wang, T. Sutton, C. Ainsworth, and F. Hernandez. 2024. "Simulating Productivity Changes of Epipelagic, Mesopelagic, and Bathypelagic Taxa Using a Depth-Resolved, End-to-End Food Web Model for the Oceanic Gulf of Mexico." *Ecological Modelling* 489(January): 110623. https://doi.org/10.1016/j.ecolmodel.2024.110623.

Chi, X., J. Dierking, H.-J. Hoving, F. Lüskow, A. Denda, B. Christiansen, U. Sommer, T. Hansen, and J. Javidpour. 2021. "Tackling the Jelly Web: Trophic Ecology of Gelatinous Zooplankton in Oceanic Food Webs of the Eastern Tropical Atlantic Assessed by Stable Isotope Analysis." *Limnology and Oceanography* 66(2): 289–305. https://doi.org/10.1002/lno.11605.

Childress, J. J., S. M. Taylor, G. M. Cailliet, and M. H. Price. 1980. "Patterns of Growth, Energy Utilization and Reproduction in Some Meso- and Bathypelagic Fishes off Southern California." *Marine Biology* 61(1): 27–40. https://doi.org/10.1007/BF00410339.

Cohen, J. E., T. Jonsson, and S. R. Carpenter. 2003. "Ecological Community Description Using the Food Web, Species Abundance, and Body Size." *Proceedings of the National Academy of Sciences of the United States of America* 100(4): 1781–86. https://doi.org/10.1073/pnas.232715699.

Cole, J. J., S. Findlay, and M. L. Pace. 1988. "Bacterial Production in Fresh and Saltwater Ecosystems: A Cross-System Overview." *Marine Ecology Progress Series* 43: 1–10. https://doi.org/10.3354/meps043001.

Cornils, A., K. Thomisch, J. Hase, N. Hildebrandt, H. Auel, and B. Niehoff. 2022. "Testing the Usefulness of Optical Data for Zooplankton Long-Term Monitoring: Taxonomic Composition, Abundance, Biomass, and Size Spectra from ZooScan Image Analysis." *Limnology and Oceanography: Methods* 20(7): 428–450. https://doi.org/10.1002/lom3.10495.

Couret, M., J. M. Landeira, V. M. Tuset, A. N. Sarmiento-Lezcano, P. Vélez-Belchí, and S. Hernández-León. 2023. "Mesozooplankton Size Structure in the Canary Current System." *Marine Environmental Research* 188(March): 105976. https://doi.org/10.1016/j.marenvres.2023.105976.

Czudaj, S., R. Koppelmann, C. Möllmann, M. Schaber, and H. O. Fock. 2021. "Community Structure of Mesopelagic Fishes Constituting Sound Scattering Layers in the Eastern Tropical North Atlantic." *Journal of Marine Systems* 224(December 2020): 103635. https://doi.org/10.1016/j.jmarsys.2021.103635.

da Silva, A., et al. 2021. "Surface Circulation and Vertical Structure of Upper Ocean Variability around Fernando de Noronha Archipelago and Rocas Atoll during Spring 2015 and Fall 2017." *Frontiers in Marine Science* 8: 598101. https://doi.org/10.3389/fmars.2021.598101.

Davison, P. C., D. M. Checkley, Jr., J. A. Koslow, and J. Barlow. 2013. "Carbon Export Mediated by Mesopelagic Fishes in the Northeast Pacific Ocean." *Progress in Oceanography* 116: 14–30. https://doi.org/10.1016/j.pocean.2013.05.013.

Davison, P., A. Lara-Lopez, and J. Anthony Koslow. 2015. "Mesopelagic Fish Biomass in the Southern California Current Ecosystem." *Deep-Sea Research Part II: Topical Studies in*

Oceanography 112(June): 129–142. https://doi.org/10.1016/j.dsr2.2014.10.007.

de Figueiredo, G. G. A. A., S. M. de Albuquerque Lira, A. Bertrand, S. Neumann-Leitão, and R. Schwamborn. 2025. "Zooplankton Abundance and Biovolume Size-Spectra in the Western Tropical Atlantic - from the Shelf towards Complex Oceanic Current Systems." *Marine Environmental Research* 204(December 2024): 106906. https://doi.org/10.1016/j.marenvres.2024.106906.

Del Giorgio, P. A., and R. L. France. 1996. "Ecosystem-Specific Patterns in the Relationship between Zooplankton and POM or Microplankton δ13C." *Limnology and Oceanography* 41(2): 359–365. https://doi.org/10.4319/lo.1996.41.2.0359.

Del Giorgio, P. A., and J. M. Gasol. 1995. "Biomass Distribution in Freshwater Plankton Communities." *American Naturalist* 146(1): 135–152. https://doi.org/10.1086/285790.

Devol, A. H., and H. E. Hartnett. 2001. "Role of the Oxygen-Deficient Zone in Transfer of Organic Carbon to the Deep Ocean." *Limnology and Oceanography* 46(7): 1684–90.

dos Santos, R. M., P. J. Hilbers, and J. A. Hendriks. 2017. "Evaluation of Models Capacity to Predict Size Spectra Parameters in Ecosystems under Stress." *Ecological Indicators* 79(April): 114–121. https://doi.org/10.1016/j.ecolind.2017.04.017.

Dossa, A. N., A. C. Silva, A. Chaigneau, G. Eldin, M. Araujo, and A. Bertrand. 2021. "Near-Surface Western Boundary Circulation off Northeast Brazil." *Progress in Oceanography* 190(October 2020): 102475. https://doi.org/10.1016/j.pocean.2020.102475.

Dugenne, M., M. Corrales-Ugalde, J. Y. Luo, R. Kiko, T. D. O'Brien, J.-O. Irisson, F. Lombard, et al. 2024. "First Release of the Pelagic Size Structure Database: Global Datasets of Marine Size Spectra Obtained from Plankton Imaging Devices." *Earth System Science Data Discussions* 16(December): 2971–99.

Dumont, H. J. 2007. "Rotifers, the Jelly Plankton of Freshwater." *Hydrobiologia* 593(1): 59–66. https://doi.org/10.1007/s10750-007-9047-8.

Duncan, S. E., A. F. Sell, W. Hagen, and H. O. Fock. 2022. "Environmental Drivers of Upper Mesopelagic Fish Assemblages in the Benguela Upwelling Systems during Austral Summer." *Marine Ecology Progress Series* 688: 133–152.

Eddy, T. D., J. R. Bernhardt, J. L. Blanchard, W. W. L. Cheung, M. Colléter, H. du Pontavice, E. A. Fulton, et al. 2021. "Energy Flow through Marine Ecosystems: Confronting Transfer Efficiency." *Trends in Ecology and Evolution* 36(1): 76–86. https://doi.org/10.1016/j.tree.2020.09.006.

Eduardo, L. N., A. Bertrand, F. Lucena-Frédou, B. T. Villarins, J. R. Martins, G. V. F. Afonso, T. W. Pietsch, T. Frédou, F. di Dario, and M. M. Mincarone. 2022. "Rich and Underreported: First Integrated Assessment of the Diversity of Mesopelagic Fishes in the Southwestern Tropical Atlantic." *Frontiers in Marine Science* 9(August): 937154. https://doi.org/10.3389/fmars.2022.937154.

Edwards, A. M., J. P. W. Robinson, M. J. Plank, J. K. Baum, and J. L. Blanchard. 2017. "Testing and Recommending Methods for Fitting Size Spectra to Data." *Methods in Ecology and Evolution* 8(1): 57–67. https://doi.org/10.1111/2041-210X.12641.

Ekau, W., H. Auel, W. Hagen, R. Koppelmann, N. Wasmund, K. Bohata, F. Buchholz, et al. 2018. "Pelagic Key Species and Mechanisms Driving Energy Flows in the Northern Benguela Upwelling Ecosystem and Their Feedback into Biogeochemical Cycles." *Journal of Marine Systems* 188(April): 49–62. https://doi.org/10.1016/j.jmarsys.2018.03.001.

Engel, A., H. Wagner, F. A. C. le Moigne, and S. T. Wilson. 2017. "Particle Export Fluxes to the Oxygen Minimum Zone of the Eastern Tropical North Atlantic." *Biogeosciences* 14: 1825–38. https://doi.org/10.5194/bg-14-1825-2017.

Flynn, B. A., A. J. Richardson, A. S. Brierley, D. C. Boyer, B. E. Axelsen, L. Scott, N. E. Moroff, P. I. Kainge, B. M. Tjizoo, and M. J. Gibbons. 2012. "Temporal and Spatial Patterns in the Abundance of Jellyfish in the Northern Benguela Upwelling Ecosystem and Their Link to Thwarted Pelagic Fishery Recovery." *African Journal of Marine Science* 34(1): 131–146. https://doi.org/10.2989/1814232X.2012.675122.

Fock, H. O., H. Andresen, A. Bertrand, G. Bitencourt, C. Carre, M. Couret Huertas, J. Díaz Pérez, et al. 2024. "Synthetic Pelagic Biomass Size Spectra of the Tropical and Subtropical Atlantic - Biovolume and Carbon Biomass Data." Zenodo. https://doi.org/10.5281/zenodo.13627093

Fock, H. O., H. Andresen, J. D. Pérez, T. Dudeck, G. Figueiredo, T. Frédou, D. Y. Ghebrehiwet, et al. 2025. "Seasonal Changes of Size Spectra of the Benguela Offshore Mesopelagic Ecosystem Compartment in Relation to Primary Production." *Marine Ecology* 46(4): e70040. https://doi.org/10.1111/maec.70040.

Fock, H. O., and S. Czudaj. 2019. "Size Structure Changes of Mesopelagic Fishes and Community Biomass Size Spectra along a Transect from the Equator to the Bay of Biscay Collected in 1966-1979 and 2014-2015." *ICES Journal of Marine Science* 76: 755–770. https://doi.org/10.1093/icesjms/fsy068.

Fock, H. O., and S. Ehrich. 2010. "Deep-Sea Pelagic Nekton Biomass Estimates in the North Atlantic: Horizontal and Vertical Resolution of Revised Data from 1982 and 1983." *Journal of Applied Ichthyology* 26: 85–101.

Gaedke, U. 1992. "The Size Distribution of Plankton Biomass in a Large Lake and its Seasonal Variability." *Limnology and Oceanography* 37(6): 1202–20. https://doi.org/10.4319/lo.1992.37.6.1202.

Gaedke, U. 1993. "Ecosystem Analysis Based on Biomass Size Distributions: A Case Study of a Plankton Community in a Large Lake." *Limnology and Oceanography* 38(1): 112–127. https://doi.org/10.4319/lo.1993.38.1.0112.

Gasol, J. M., D. Giorgio, A. Paul, and C. M. Duarte. 1997. "Biomass Distribution in Marine Planktonic Communities." *Limnology and Oceanography* 42(6): 1353–63. https://doi.org/10.4319/lo.1997.42.6.1353.

Giacomini, H. C., D. T. de Kerckhove, V. Kopf, and C. Chu. 2023. "Statistical Modelling of Aquatic Size Spectra: Integrating Data from Multiple Taxa and Sampling Methods." *Aquatic Ecosystem Health & Management* 26(3): 17–25. https://doi.org/10.14321/aehm.026.03.17.

Glazier, D. S. 2014. "Metabolic Scaling in Complex Living Systems." *Systems* 2(4): 451–540. https://doi.org/10.3390/systems2040451.

Gloeckler, K., C. A. Choy, C. C. S. Hannides, H. G. Close, E. Goetze, B. N. Popp, and J. C. Drazen. 2018. "Stable Isotope Analysis of Micronekton around Hawaii Reveals Suspended Particles Are an Important Nutritional Source in the Lower Mesopelagic and Upper Bathypelagic Zones." *Limnology and Oceanography* 63(3): 1168–80. https://doi.org/10.1002/lno.10762.

Gómez-Canchong, P., J. M. Blanco, and R. A. Quiñones. 2013. "On the Use of Biomass Size Spectra Linear Adjustments to Design Ecosystem Indicators." *Scientia Marina* 77(2): 257–268. https://doi.org/10.3989/scimar.03708.22A.

González-García, C., S. Agustí, J. Aiken, A. Bertrand, G. Bittencourt Farias, A. Bode, C. Carré, et al. 2023. "Basin-Scale Variability in Phytoplankton Size-Abundance Spectra across the Atlantic Ocean." *Progress in Oceanography* 217(March): 103104. https://doi.org/10.1016/j.pocean.2023.103104.

Grossart, H. P., and M. Simon. 1998. "Significance of Limnetic Organic Aggregates (Lake Snow) for the Sinking Flux of Particulate Organic Matter in a Large Lake." *Aquatic Microbial Ecology* 15(2): 115–125. https://doi.org/10.3354/ame015115.

Grossart, H.-P.-P., and M. Simon. 1993. "Limnetic Macroscopic Organic Aggregates (Lake Snow): Occurrence, Characteristics, and Microbial Dynamics in Lake Constance." *Limnology and Oceanography* 38(3): 532–546. https://doi.org/10.4319/lo.1993.38.3.0532.

Guiet, J., J. C. Poggiale, and O. Maury. 2016. "Modelling the Community Size-Spectrum: Recent Developments and New Directions." *Ecological Modelling* 337: 4–14. https://doi.org/10.1016/j.ecolmodel.2016.05.015.

Hansman, R. L., and A. L. Sessions. 2016. "Measuring the In Situ Carbon Isotopic Composition of Distinct Marine Plankton Populations Sorted by Flow Cytometry." *Limnology and Oceanography: Methods* 14(2): 87–99. https://doi.org/10.1002/lom3.10073.

Hatton, I. A., R. F. Heneghan, Y. M. Bar-On, and E. D. Galbraith. 2021. "The Global Ocean Size Spectrum from Bacteria to Whales." *Science Advances* 7(46): eabh3732. https://doi.org/10.1126/sciadv.abh3732.

Havens, K. E., A. Kirsten, and T. L. East. 2000. "Relative Efficiencies of Carbon Transfer from Bacteria and Algae to Zooplankton in a Subtropical Lake." *Journal of Plankton Research* 22(9): 1801–9.

Heath, M. R. 1995. "Size Spectrum Dynamics and the Planktonic Ecosystem of Loch Linnhe." *ICES Journal of Marine Science* 52(3–4): 627–642. https://doi.org/10.1016/1054-3139(95)80077-8.

Hoving, H. J. T., P. Neitzel, H. Hauss, S. Christiansen, R. Kiko, B. H. Robison, P. Silva, and A. Körtzinger. 2020. "In Situ Observations Show Vertical Community Structure of Pelagic Fauna in the Eastern Tropical North Atlantic off Cape Verde." *Scientific Reports* 10(1): 21798. https://doi.org/10.1038/s41598-020-78255-9.

Huete-Ortega, M., P. Cermeño, A. Calvo-Díaz, and E. Marañón. 2011. "Isometric Size-Scaling of Metabolic Rate and the Size Abundance Distribution of Phytoplankton." *Proceedings of the Royal Society B: Biological Sciences* 279(1734): 1815–23. https://doi.org/10.1098/rspb.2011.2257.

Hunt, B. P. V., V. Allain, C. Menkes, A. Lorrain, B. Graham, M. Rodier, M. Pagano, and F. Carlotti. 2015. "A Coupled Stable Isotope-Size Spectrum Approach to Understanding Pelagic Food-Web Dynamics: A Case Study from the Southwest Sub-Tropical Pacific." *Deep-Sea Research Part II: Topical Studies in Oceanography* 113: 208–224. https://doi.org/10.1016/j.dsr2.2014.10.023.

Iversen, M. H. 2023. "Carbon Export in the Ocean: A Biologist's Perspective." *Annual Review of Marine Science* 15: 357–381.

Jaspers, C., R. R. Hopcroft, T. Kiørboe, F. Lombard, Á. López-Urrutia, J. D. Everett, and A. J. Richardson. 2023. "Gelatinous Larvacean Zooplankton Can Enhance Trophic Transfer and Carbon Sequestration." *Trends in Ecology and Evolution* 38(10): 980–993. https://doi.org/10.1016/j.tree.2023.05.005.

Jennings, S., and S. Mackinson. 2003. "Abundance-Body Mass Relationships in Size-Structured Food Webs." *Ecology Letters* 6(11): 971–74. https://doi.org/10.1046/j.1461-0248.2003.00529.x.

Kang, H. C., H. J. Jeong, J. H. Ok, A. S. Lim, K. Lee, J. H. You, S. A. Park, et al. 2023. "Food Web Structure for High Carbon Retention in Marine Plankton Communities." *Science Advances* 9(50): eadk0842. https://doi.org/10.1126/sciadv.adk0842.

Kaschner, K., J. S. Ready, E. Agbayani, J. Rius, K. Kesner-Reyes, P. D. Eastwood, A. B. South, et al. 2008. AquaMaps Environmental Dataset: Half-Degree Cells Authority File (HCAF) www.aquamaps.org/data

Kerr, S. R., and L. M. Dickie. 2001. *The Biomass Spectrum*. New York: Columbia University Press.

Kiko, R., H. Hauss, M. Picheral, and L. Stemmann. 2017. "Abundance of Particles Measured with an Underwater Vision Profiler 5 (UVP5) During Maria S. Merian Cruise MSM22" PANGAEA. https://doi.org/10.1594/PANGAEA.874871

Kiko, R., M. Picheral, D. Antoine, M. Babin, L. Berline, T. Biard, E. Boss, et al. 2022. "A Global Marine Particle Size Distribution Dataset Obtained with the Underwater Vision Profiler 5." *Earth System Science Data* 14(9): 4315–37. https://doi.org/10.5194/essd-14-4315-2022.

Knorrn, A. H., K. L. Wieben, H. O. Fock, and H. Andresen. 2024. "Reproductive Biology of the Electric Lanternfish Electrona Risso (Myctophidae) and the Bigscale Fishes *Melamphaes polylepis* and *Scopelogadus mizolepis* (Melamphaidae)." *Journal of Fish Biology* 104(September): 252–264. https://doi.org/10.1111/jfb.15575.

Kwong, L. E., T. Ross, F. Lüskow, K. R. N. Florko, and E. A. Pakhomov. 2022. "Spatial, Seasonal, and Climatic Variability in Mesozooplankton Size Spectra along a Coastal-to-Open Ocean Transect in the Subarctic Northeast Pacific." *Progress in Oceanography* 201: 102728. https://doi.org/10.1016/j.pocean.2021.102728.

Lehodey, P., R. Murtugudde, and I. Senina. 2010. "Bridging the Gap from Ocean Models to Population Dynamics of Large Marine Predators: A Model of Mid-Trophic Functional Groups." *Progress in Oceanography* 84(1–2): 69–84. https://doi.org/10.1016/j.pocean.2009.09.008.

Lenth, R. 2024. "emmeans: Estimated Marginal Means, aka Least-Squares Means." R Package Version 1.10.2.

Lira, S. M. A., R. Schwamborn, M. d. Melo Júnior, H. L. Varona, S. Queiroz, D. Veleda, A. J. Silva, S. Neumann-Leitão, M. Araujo, and C. R. Marcolin. 2024. "Multiple Island Effects Shape

Oceanographic Processes and Zooplankton Size Spectra Off an Oceanic Archipelago in the Tropical Atlantic." *Journal of Marine Systems* 242(October 2023): 103942. https://doi.org/10.1016/j.jmarsys.2023.103942.

Lombard, F., G. Lionel, M. C. Brandão, C. L. Pedro, C. Sébastien, P. D. J. Richard, E. Amanda, et al. 2024. "Ubiquity of Inverted 'Gelatinous' Ecosystem Pyramids in the Global Ocean." bioRxiv (urtarrilak 1): 2024.02.09.579612. https://doi.org/10.1101/2024.02.09.579612

Longhurst, A. 2007. *Ecological Geography of the Sea*. San Diego: Academic Press.

Lotze, H. K., D. P. Tittensor, A. Bryndum-Buchholz, T. D. Eddy, W. W. L. Cheung, E. D. Galbraith, M. Barange, et al. 2019. "Global Ensemble Projections Reveal Trophic Amplification of Ocean Biomass Declines with Climate Change." *Proceedings of the National Academy of Sciences of the United States of America* 116(26): 12907–12. https://doi.org/10.1073/pnas.1900194116.

Lüskow, F., N. Bezio, L. Caputo, X. Chi, H. J. Dumont, K. D. Karunarathne, P. J. López-González, et al. 2024. "Hidden Gems: Scattered Knowledge Hampered Freshwater Jellyfish Research over the Past One-and-a-Half Centuries." *Ecology and Evolution* 14(10): e70350. https://doi.org/10.1002/ece3.70350.

Marañón, E., P. Cermeóo, J. Rodríguez, M. V. Zubkov, and R. P. Harris. 2007. "Scaling of Phytoplankton Photosynthesis and Cell Size in the Ocean." *Limnology and Oceanography* 52(5): 2190–98. https://doi.org/10.4319/lo.2007.52.5.2190.

Marañón, E., F. van Wambeke, J. Uitz, E. S. Boss, C. Dimier, J. Dinasquet, A. Engel, et al. 2021. "Deep Maxima of Phytoplankton Biomass, Primary Production and Bacterial Production in the Mediterranean Sea." *Biogeosciences* 18(5): 1749–67. https://doi.org/10.5194/bg-18-1749-2021.

Marohn, L., M. Schaber, M. Freese, J. D. Pohlmann, K. Wysujack, S. Czudaj, T. Blancke, and R. Hanel. 2021. "Distribution and Diel Vertical Migration of Mesopelagic Fishes in the Southern Sargasso Sea—Observations Through Hydroacoustics and Stratified Catches." *Marine Biodiversity* 51(6): 87. https://doi.org/10.1007/s12526-021-01216-6.

Martens, E. A., N. Wadhwa, N. S. Jacobsen, C. Lindemann, K. H. Andersen, and A. Visser. 2015. "Size Structures Sensory Hierarchy in Ocean Life." *Proceedings of the Royal Society B: Biological Sciences* 282(1815): 20151346. https://doi.org/10.1098/rspb.2015.1346.

Martin, B., H. Auel, M. Bode-Dalby, T. Dudeck, S. Duncan, W. Ekau, H. O. Fock, et al. 2024. "Studies of the Ecology of the Benguela Current Upwelling System-the TRAFFIC 1 Approach." In *Sustainability of Southern African Ecosystems under Global Change - Science for Management and Policy Interventions*, edited by G. P. von Maltitz, 277–312. Cham: Springer International Publishing.

Martin, E. S., R. P. Harris, and X. Irigoien. 2006. "Latitudinal Variation in Plankton Size Spectra in the Atlantic Ocean." *Deep Sea Research II* 53: 1560–72. https://doi.org/10.1016/j.dsr2.2006.05.006.

Maury, O. 2010. "An Overview of APECOSM, a Spatialized Mass Balanced 'Apex Predators ECOSystem Model' to Study Physiologically Structured Tuna Population Dynamics in Their Ecosystem." *Progress in Oceanography* 84(1–2): 113–17. https://doi.org/10.1016/j.pocean.2009.09.013.

McCallister, S. L., D. Giorgio, and A. Paul. 2008. "Direct Measurement of the δ13C Signature of Carbon Respired by Bacteria in Lakes: Linkages to Potential Carbon Sources, Ecosystem Baseline Metabolism, and CO_2 Fluxes." *Limnology and Oceanography* 53(4): 1204–16. https://doi.org/10.4319/lo.2008.53.4.1204.

Mehner, T., K. Attermeyer, M. Brauns, S. Brothers, S. Hilt, K. Scharnweber, R. M. van Dorst, M. J. Vanni, and U. Gaedke. 2022. "Trophic Transfer Efficiency in Lakes." *Ecosystems* 25(8): 1628–52. https://doi.org/10.1007/s10021-022-00776-3.

Mehner, T., B. Lischke, K. Scharnweber, K. Attermeyer, S. Brothers, U. Gaedke, S. Hilt, and S. Brucet. 2018. "Empirical Correspondence between Trophic Transfer Efficiency in Freshwater Food Webs and the Slope of Their Size Spectra." *Ecology* 99(6): 1463–72. https://doi.org/10.1002/ecy.2347.

Merrett, N. R. 1994. "Reproduction in the North Atlantic Oceanic Ichthyofauna and the Relationship between Fecundity and Species' Sizes." *Environmental Biology of Fishes* 41(1–4): 207–245. https://doi.org/10.1007/bf00023814.

Midway, S., M. Robertson, S. Flinn, and M. Kaller. 2020. "Comparing Multiple Comparisons: Practical Guidance for Choosing the Best Multiple Comparisons Test." *PeerJ* 8: e10387. https://doi.org/10.7717/peerj.10387.

Moigne, F. A. C. L., C. Cisternas-Novoa, J. Piontek, M. Maßmig, and A. Engel. 2017. "On the Effect of Low Oxygen Concentrations on Bacterial Degradation of Sinking Particles." *Scientific Reports* 7(September 2016): 16722. https://doi.org/10.1038/s41598-017-16903-3.

Moreno-Ostos, E., J. M. Blanco, S. Agustí, L. M. Lubián, V. Rodríguez, R. L. Palomino, M. Llabrés, and J. Rodríguez. 2015. "Phytoplankton Biovolume Is Independent from the Slope of the Size Spectrum in the Oligotrophic Atlantic Ocean." *Journal of Marine Systems* 152: 42–50. https://doi.org/10.1016/j.jmarsys.2015.07.008.

Olivar, M. P., P. A. Hulley, A. Castellón, M. Emelianov, C. López, V. M. Tuset, T. Contreras, and B. Molí. 2017. "Mesopelagic Fishes across the Tropical and Equatorial Atlantic: Biogeographical and Vertical Patterns." *Progress in Oceanography* 151: 116–137. https://doi.org/10.1016/j.pocean.2016.12.001.

Otto, S. B., B. C. Rall, and U. Brose. 2007. "Allometric Degree Distributions Facilitate Food-Web Stability." *Nature* 450(7173): 1226–29. https://doi.org/10.1038/nature06359.

Padfield, D., A. Buckling, R. Warfield, C. Lowe, and G. Yvon-Durocher. 2018. "Linking Phytoplankton Community Metabolism to the Individual Size Distribution." *Ecology Letters* 21(8): 1152–61. https://doi.org/10.1111/ele.13082.

Paternoster, R., R. Brame, P. Mazerolle, and A. Piquero. 1998. "Using the Correct Statistical Test for the Equality of Regression Coefficients." *Criminology* 36: 859–866.

Pauly, D., and V. Christensen. 1995. "Primary Production Required to Sustain Global Fisheries." *Nature* 374(6519): 255–57. https://doi.org/10.1038/374255a0.

Pérez, V., E. Fernández, E. Marañón, P. Serret, and C. García-Soto. 2005. "Seasonal and Interannual Variability of Chlorophyll a and Primary Production in the Equatorial Atlantic: In Situ and Remote Sensing Observations." *Journal of Plankton Research* 27(2): 189–197. https://doi.org/10.1093/plankt/fbh159.

Picaut, J., J. Servain, A. J. Busalacchi, and M. Seva. 1984. "Interannual Variability Versus Seasonal Variability in the Tropical Atlantic." *Geophysical Research Letters* 11(8): 787–790. https://doi.org/10.1029/GL011i008p00787.

Pinheiro, J., et al. 2021. "nlme: Linear and Nonlinear Mixed Effects Models." https://cran.r-project.org/package=nlme.

Pitt, K. A., C. M. Duarte, C. H. Lucas, K. R. Sutherland, R. H. Condon, H. Mianzan, J. E. Purcell, K. L. Robinson, and S.-I. Uye. 2013. "Jellyfish Body Plans Provide Allometric Advantages beyond Low Carbon Content." *PLoS One* 8(8): e72683. https://doi.org/10.1371/journal.pone.0072683.

Platt, T., and K. Denman. 1977. "Organisation in the Pelagic Ecosystem." *Helgoländer Wissenschaftliche Meeresuntersuchungen* 30(1–4): 575–581. https://doi.org/10.1007/BF02207862.

Platt, T., and S. Sathyendranath. 1999. "Spatial Structure of Pelagic Ecosystem Processes in the Global Ocean." *Ecosystems* 2(5): 384–394. https://doi.org/10.1007/s100219900088.

Pomeroy, L. R., et al. 2007. "The Microbial Loop." *Oceanography* 20(Spl.Iss. 2): 28–33. https://doi.org/10.5670/oceanog.2007.45.

Quinones, R. A., T. Platt, and J. Rodríguez. 2003. "Patterns of Biomass-Size Spectra from Oligotrophic Waters of the Northwest Atlantic." *Progress in Oceanography* 57(3–4): 405–427. https://doi.org/10.1016/s0079-6611(03)00108-3.

R Development Core Team. 2023. *R: A Language and Environment for Statistical Computing*. Vienna: R Foundation for Statistical Computing.

Rodríguez, J. 1994. "Some Comments on the Size-Based Structural Analysis of the Pelagic Ecosystem." *Scientia Marina* 58(2): 1–10. http://www.icm.csic.es/scimar/pdf/58/sm58n1001.pdf.

Roshan, S., and T. DeVries. 2017. "Efficient Dissolved Organic Carbon Production and Export in the Oligotrophic Ocean." *Nature Communications* 8(1): 2036. https://doi.org/10.1038/s41467-017-02227-3.

Rossberg, A. G., U. Gaedke, and P. Kratina. 2019. "Dome Patterns in Pelagic Size Spectra Reveal Strong Trophic Cascades." *Nature Communications* 10(1): 4396. https://doi.org/10.1038/s41467-019-12289-0.

Roux, J. P., C. D. van der Lingen, M. J. Gibbons, N. E. Moroff, L. J. Shannon, A. D. M. Smith, and P. M. Cury. 2013. "Jellyfication of Marine Ecosystems as a Likely Consequence of Overfishing Small Pelagic Fishes: Lessons from the Benguela." *Bulletin of Marine Science* 89(1): 249–284. https://doi.org/10.5343/bms.2011.1145.

Sameoto, D., P. Wiebe, J. Runge, L. Postel, J. Dunn, C. Miller, and S. Coombs. 2000. "Collecting Zooplankton." In *ICES Zooplankton Methodology Manual*, edited by R. Harris, P. Wiebe, and M. Huntley, 55–81. London: Academic Press. https://doi.org/10.1016/B978-012327645-2/50004-9.

Searle, S. R., F. M. Speed, and G. A. Milliken. 1980. "Population Marginal Means in the Linear Model: An Alternative to Least Squares Means." *The American Statistician* 34(4): 216–221.

Sheldon, R. W., and T. R. Parsons. 1967. "A Continuos Size Spectrum for Particulate Matter in the Sea." *Journal of the Fisheries Research Board of Canada* 24(July 1966): 909–915.

Sheldon, R. W., A. Prakash, and H. Sutcliffe. 1972. "The Size Distribution of Particles in the Ocean." *Limnology and Oceanography* XVII (MAY): 327–340.

Sheldon, R. W., W. H. Sutcliffe, Jr., and M. A. Paranjape. 1977. "Structure of Pelagic Food Chain and Relationship between Plankton and Fish Production." *Journal of the Fisheries Research Board of Canada* 34(12): 2344–53. https://doi.org/10.1139/f77-314.

Silvert, W., and T. Platt. 1978. "Energy Flux in the Pelagic Ecosystem: A Time-Dependent Equation." *Limnology and Oceanography* 23(4): 813–16.

Simon, M., B. C. Cho, and F. Azam. 1992. "Significance of Bacterial Biomass in Lakes and the Ocean: Comparison to Phytoplankton Biomass and Biogeochemical Implications." *Marine Ecology Progress Series* 86(2): 103–110. https://doi.org/10.3354/meps086103.

Soviadan, Y. D., F. Benedetti, M. C. Brandão, S.-D. Ayata, J.-O. Irisson, J. L. Jamet, R. Kiko, F. Lombard, K. Gnandi, and L. Stemmann. 2022. "Patterns of Mesozooplankton Community Composition and Vertical Fluxes in the Global Ocean." *Progress in Oceanography* 200(urtarrilak): 102717. https://doi.org/10.1101/2021.07.20.452978, http://biorxiv.org/content/early/2021/07/20/2021.07.20.452978.abstract.

Soviadan, Y. D., M. Dugenne, L. Drago, T. Biard, E. Trudnowska, F. Lombard, J.-B. Romagnan, et al. 2024. "Combining In Situ and Ex Situ Plankton Image Data to Reconstruct Zooplankton (>1 mm) Volume and Mass Distribution in the Global Ocean." *Journal of Plankton Research* 46(5): 461–474. https://doi.org/10.1093/plankt/fbae046.

Spalding, M. D., V. N. Agostini, J. Rice, and S. M. Grant. 2012. "Pelagic Provinces of the World: A Biogeographic Classification of the World's Surface Pelagic Waters." *Ocean and Coastal Management* 60: 19–30. https://doi.org/10.1016/j.ocecoaman.2011.12.016.

Sprules, W. G., and L. E. Barth. 2015. "Surfing the Biomass Size Spectrum: Some Remarks on History, Theory, and Application." *Canadian Journal of Fisheries and Aquatic Sciences* 73(4): 477–495. https://doi.org/10.1139/cjfas-2015-0115.

Sprules, W. G., and A. P. Goyke. 1994. "Size-Based Structure and Production in the Pelagia of Lakes Ontario and Michigan." *Canadian Journal of Fisheries and Aquatic Sciences* 51(11): 2603–11. https://doi.org/10.1139/f94-260.

Stemmann, L., and E. S. Boss. 2012. "Plankton and Particle Size and Packaging: From Determining Optical Properties to Driving the Biological Pump." *Annual Review of Marine Science* 4: 263–290.

Straile, D. 1997. "Gross Growth Efficiencies of Protozoan and Metazoan Zooplankton and their Dependence on Food Concentration, Predator-Prey Weight Ratio, and Taxonomic Group." *Limnology and Oceanography* 42(6): 1375–85. https://doi.org/10.4319/lo.1997.42.6.1375.

Stramma, L., G. C. Johnson, J. Sprintall, and V. Mohrholz. 2008. "Expanding Oxygen-Minimum Zones in the Tropical Oceans." *Science* 320: 655–58.

Stukel, M. R., M. Décima, T. B. Kelly, M. R. Landry, S. D. Nodder, M. D. Ohman, K. E. Selph, and N. Yingling. 2024. "Relationships between Plankton Size Spectra, Net Primary Production, and the Biological Carbon Pump." *Global Biogeochemical Cycles* 38(4): 1–14. https://doi.org/10.1029/2023GB007994.

Sutton, T. T., M. R. Clark, D. C. Dunn, P. N. Halpin, A. D. Rogers, J. Guinotte, S. J. Bograd, et al. 2017. "A Global Biogeographic Classification of the Mesopelagic Zone." *Deep-Sea Research*

Part I: Oceanographic Research Papers 126(May): 85–102. https://doi.org/10.1016/j.dsr.2017.05.006.

Thiebaux, M. L., and L. M. Dickie. 1992. "Models of Aquatic Biomass Size Spectra and the Common Structure of their Solutions." *Journal of Theoretical Biology* 159(2): 147–161. https://doi.org/10.1016/S0022-5193(05)80699-X.

Thiebaux, M. L., and L. M. Dickie. 1993. "Structure of the Body-Size Spectrum of the Biomass in Aquatic Ecosystems: A Consequence of Allometry in Predator-Prey Interactions." *Canadian Journal of Fisheries and Aquatic Sciences* 50(6): 1308–17. https://doi.org/10.1139/f93-148.

Tosetto, E. G., A. Bertrand, S. Neumann-Leitão, A. Costa da Silva, and M. Nogueira Júnior. 2021. "Spatial Patterns in Planktonic Cnidarian Distribution in the Western Boundary Current System of the Tropical South Atlantic Ocean." *Journal of Plankton Research* 43(2): 270–287. https://doi.org/10.1093/plankt/fbaa066.

Trebilco, R., J. K. Baum, A. K. Salomon, and N. K. Dulvy. 2013. "Ecosystem Ecology: Size-Based Constraints on the Pyramids of Life." *Trends in Ecology and Evolution* 28(7): 423–431. https://doi.org/10.1016/j.tree.2013.03.008.

Vihtakari, M. 2024. "ggOceanMaps: Plot Data on Oceanographic Maps Using 'ggplot2'." https://mikkovihtakari.github.io/ggOceanMaps/.

Witek, Z., and A. Krajewska-Soltys. 1989. "Some Examples of the Epipelagic Plankton Size Structure in High Latitude Oceans." *Journal of Plankton Research* 11(6): 1143–55. https://doi.org/10.1093/plankt/11.6.1143.

Yang, G., C. Li, K. Guilini, X. Wang, and Y. Wang. 2017. "Regional Patterns of δ13C and δ15N Stable Isotopes of Size-Fractionated Zooplankton in the Western Tropical North Pacific Ocean." *Deep-Sea Research Part I: Oceanographic Research Papers* 120(December 2016): 39–47. https://doi.org/10.1016/j.dsr.2016.12.007.

Yurista, P. M., D. L. Yule, M. Balge, J. D. VanAlstine, J. A. Thompson, A. E. Gamble, T. R. Hrabik, J. R. Kelly, J. D. Stockwell, and M. R. Vinson. 2014. "A New Look at the Lake Superior Biomass Size Spectrum." *Canadian Journal of Fisheries and Aquatic Sciences* 71(9): 1324–33. https://doi.org/10.1139/cjfas-2013-0596.

Yvon-Durocher, G., J. Reiss, J. Blanchard, B. Ebenman, D. M. Perkins, D. C. Reuman, A. Thierry, G. Woodward, and O. L. Petchey. 2011. "Across Ecosystem Comparisons of Size Structure: Methods, Approaches and Prospects." *Oikos* 120(4): 550–563. https://doi.org/10.1111/j.1600-0706.2010.18863.x.

Zhou, M., and M. E. Huntley. 1997. "Population Dynamics Theory of Plankton Based on Biomass Spectra." *Marine Ecology Progress Series* 159(November): 61–73. https://doi.org/10.3354/meps159061.

Zimmer, K. D., R. C. Grow, A. R. Tipp, B. R. Herwig, D. F. Staples, J. B. Cotner, and P. C. Jacobson. 2020. "Stable Isotope Patterns in Lake Food Webs Reflect Productivity Gradients." *Ecosphere* 11(9): e03244. https://doi.org/10.1002/ecs2.3244.

SUPPORTING INFORMATION

Additional supporting information can be found online in the Supporting Information section at the end of this article.

How to cite this article: Fock, Heino O., Henrike Andresen, Arnaud Bertrand, Gabriel Bittencourt Farias, Claire Carré, María Couret, Javier Díaz-Pérez, et al. 2026. "Synthetic Pelagic Biomass Size Spectra of the Tropical and Subtropical Atlantic." *Ecosphere* 17(5): e70608. https://doi.org/10.1002/ecs2.70608